

TOPICAL REVIEW

Sensing temperature via downshifting emissions of lanthanide-doped metal oxides and salts. A review

To cite this article: Miroslav D Dramianin 2016 *Methods Appl. Fluoresc.* **4** 042001


View the [article online](#) for updates and enhancements.

Related content

- [Luminescence thermometry via the two-dopant intensity ratio of Y₂O₃:Er³⁺, Eu³⁺](#)
Mihailo D Rabasovi, Branka D Muri, Vladan elebonovi et al.
- [Luminescent lanthanide reporters: new concepts for use in bioanalytical applications](#)
Johanna Vuojola and Tero Soukka
- [Self-referenced luminescence thermometry with Sm³⁺ doped TiO₂ nanoparticles](#)
M D Dramianin, Ž Anti, S ulubrk et al.


Recent citations

- [In situ 3-D temperature mapping of high average power cryogenic laser amplifiers](#)
Han Chi et al
- [Tunable emission color of Li₂ SrSiO₄:Tb³⁺ due to cross-relaxation process and optical thermometry investigation](#)
Xiao Zhou et al
- [Upconversion luminescence properties and thermal quenching mechanisms in the layered perovskite La_{1.9}Er_{0.1}Ti₂O₇ towards an application as optical temperature sensor](#)
Alexandre Bayart et al

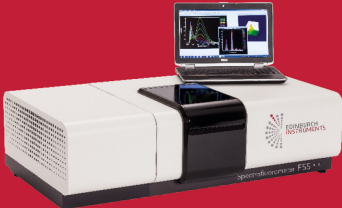


EDINBURGH INSTRUMENTS

EXPERTS in FLUORESCENCE SPECTROSCOPY



FLS1000
PHOTOLUMINESCENCE SPECTROMETER



FS5 PHOTON COUNTING SPECTROFLUOROMETER

- TIME-RESOLVED FLUORESCENCE
- STEADY STATE FLUORESCENCE
- PHOSPHORESCENCE LIFETIME
- TRANSIENT ABSORPTION

Methods and Applications in Fluorescence



TOPICAL REVIEW

Sensing temperature via downshifting emissions of lanthanide-doped metal oxides and salts. A review

RECEIVED
9 December 2015

REVISED
3 September 2016

ACCEPTED FOR PUBLICATION
12 September 2016

PUBLISHED
11 October 2016

Miroslav D Dramićanin

Vinča Institute of Nuclear Sciences, University of Belgrade, 11001 Belgrade, Serbia

E-mail: dramican@vinca.rs

Keywords: luminescence thermometry, metal oxides, rare earths, temperature, sensor, downshifting emission, phosphors

Abstract

Temperature is important because it has an effect on even the tiniest elements of daily life and is involved in a broad spectrum of human activities. That is why it is the most commonly measured physical quantity. Traditional temperature measurements encounter difficulties when used in some emerging technologies and environments, such as nanotechnology and biomedicine. The problem may be alleviated using optical techniques, one of which is luminescence thermometry. This paper reviews the state of luminescence thermometry and presents different temperature read-out schemes with an emphasis on those utilizing the downshifting emission of lanthanide-doped metal oxides and salts. The read-out schemes for temperature include those based on measurements of spectral characteristics of luminescence (band positions and shapes, emission intensity and ratio of emission intensities), and those based on measurements of the temporal behavior of luminescence (lifetimes and rise times). This review (with 140 references) gives the basics of the fundamental principles and theory that underlie the methods presented, and describes the methodology for the estimation of their performance. The major part of the text is devoted to those lanthanide-doped metal oxides and salts that are used as temperature probes, and to the comparison of their performance and characteristics.

1. Introduction

Thermometry, the practice of temperature measurements, started relatively late in human history when Galileo Galilei invented the air thermoscope sometime between the years 1592 and 1603. Developments in the eighteenth and nineteenth centuries established the forms of thermometry that are familiar today in everyday life, experimental science, and technological applications. Temperature is both a thermodynamic property and a fundamental unit of measurement; one of the seven base quantities of the international system of units (SI). It can be seen simply as the ‘degree of hotness or coldness,’ a qualitative definition built on the bodily sensation of heat and cold. Today it is readily defined from the principles of classical thermodynamics as the parameter of state that has the same value for any systems which are in thermal equilibrium, and from statistical mechanics as a direct measure of the average kinetic energy of non-interacting particles [1].

Temperature is an intensive quantity, meaning that its value does not depend on the amount of the sub-

stance for which it is measured. That temperature is not an additive quantity had exceptional implications for its measurement and the creation of temperature scale. It still has, even today, for its measurement in important emerging environments (nanoscale or intracellular, for instance) for which reliable and standardized thermometry methods have not yet been developed, contrary to the cases of many other physical quantities. Temperature is important because it is something we feel and because it has an effect on the smallest aspects of our daily life, from how to adjust our housing and clothing to what we eat for supper. It affects the life cycles of plants and animals, governs rates of chemical reactions, influences tides and so on. For these reasons, it is by far the most commonly measured physical quantity; sensors of temperature account for 80% of all sensors worldwide at present [2] and they are used across a broad spectrum of human activities, such as in medicine, home appliances, meteorology, agriculture, and industrial and military contexts, to mention some of the most significant areas.

Temperature measurements are currently conducted by many diverse measurement devices based on

assorted measurement principles. Liquid-in-glass thermometers, thermocouples and pyrometers are the most frequently utilized devices, but common thermometry also includes thermometers based on the expansion of solids, gas thermometers, manometric thermometers, resistance thermometers, semiconductor thermometers, fiber optic thermometers, quartz and ultrasonic thermometers [3]. However, emerging technologies and novel applications have presented requirements for new measurement conditions. Today, an immediate need exists for the non-contact thermometry of moving or contact-sensitive objects, difficult to access pieces, bodies in hazardous locations, objects of nanosize dimensions, or living cells and organisms. However, the properties of existing thermometers and sensor platforms limit their use in such environments. Temperature sensing based on changes in the optical properties of materials has the potential to meet many of the aforementioned needs as has been recently demonstrated by many research groups. These methods utilize the temperature dependences of Rayleigh and Raman light scattering, reflectance and refraction, but the temperature dependencies of the luminescent properties of materials have attracted the most attention. This interest is motivated by the strong sensitivity of luminescence on temperature and the ease with which luminescence can be detected in comparison to other optical signals. As the temperature of the materials changes, the luminescent characteristics, such as emission intensity, decay and rise time, and band positions and widths, may all change.

To date, various materials have been used for luminescence thermometry: semiconductors, organic dyes, polymers and organic–inorganic hybrids, but lanthanide-doped materials and nanomaterials have been the materials of choice in most instances. This is because the luminescence of lanthanide ions shows plentiful narrow emission lines and relatively long emission lifetimes in different spectral regions that can be used for temperature sensing, and also because lanthanide luminescence is prone to photobleaching and fairly influenced by materials' surroundings. In addition, lanthanide luminescence provides materials with the ability to perform multiple functions and to meet otherwise unattainable performance needs, for example, to perform intratumoral thermal reading during photothermal therapy [4]. Multifunctional (or polyvalent) luminescent materials may be constructed by adding thermometric functionality to materials already chosen for specific applications according to their other properties, or by completely new material design through a careful combination of physical properties and functional capabilities.

Considering the rapid growth of the luminescence thermometry field, it is difficult even for experts to keep abreast of new developments through the information presented in scientific and technical papers. Up-to-date summaries of the practice of luminescence thermometry that are published at regular intervals may allevi-

ate this difficulty. Until now, several comprehensive reviews [5–25] and two books [26, 27] have been published which are devoted in part or in full to the practice of temperature measurements via luminescence. Some reviews are now dated and, additionally, the field has grown considerably over the past few years making it an extremely difficult enterprise to provide an overview of all the achievements.

This review article aims to summarize developments related to temperature measurements via the downshifting emission of lanthanide ions incorporated into the metal oxides and salts. Seemingly, a small fraction of the materials used for luminescence thermometry probes, lanthanide-doped metal oxides and salts are in fact an extensive group of materials, well known for a long time and mostly used for phosphor applications. Phosphors possess exceptional properties, such as superior thermal and chemical stability, and excellent quantum efficiency of emission. Owing to these properties, the highest temperature ever measured by luminescence thermometry of 2000 K was achieved using Dy³⁺-doped Y₃Al₅O₁₂ [28]. It is worth mentioning that lanthanide-doped metal oxides and salts can be prepared in different forms: powders, crystals or ceramics by well-developed synthesis methods; this appreciably eases their adoption in luminescence thermometry. Lastly, but quite importantly, the majority of these materials allow the use of more than one temperature read-out scheme, including both self-referencing ones that will be described later in the text.

The content of the review is organized as follows. The short theoretical lead-in at the beginning of the second section aims to provide newcomers to this field with a basic understanding of lanthanide luminescence and its temperature quenching. The measurement principles and methods of luminescence thermometry are presented in a separate section. Then, the standardized ways of estimating the performance of luminescent thermometry methods are described. The largest part of the text is devoted to lanthanide-doped metal oxides and salts that are used as temperature probes on account of their downshifting emissions, as well as to the comparison of their performance and characteristics. It was not my intention to give a detailed summary of the applications since this would considerably expand the text, nevertheless, a few examples are depicted. The literature cited here is believed to cover all the relevant works published up to May, 2016.

2. Principles and methods of luminescence thermometry

Since the first human perception of light without a fire and fascination with examples from nature such as glowing worms, seashells, Aurora Borealis and the like, through the discovery of Bologna stone at the beginning of the 17th century, to the present-day use of lasers, lighting, displays and biolabels, the interest in understanding and using luminescence has been

growing continuously. The term luminescence is used today to describe the phenomenon in which the electronic state of a substance is excited by some kind of external energy and the excitation energy is released as photons in the ultraviolet, visible and near-infrared spectral regions [29]. Among many types of luminescence, the one that originates from lanthanide ions has received special attention and found important applications. Lanthanides (Ln) are 15 elements that belong to the sixth row of the periodic table of elements, from La (atomic number 57) to Lu (atomic number 71). The valence electrons of lanthanides are linked with the 4f orbital which is shielded from external electric fields by the outer 5s² and 5p⁶ electrons. Electron transitions between 4f states are forbidden according to Laporte's selection rule; however, when lanthanide ions are surrounded by a non-symmetric local environment, the f–f transitions become partially allowed. For this reason, f–f luminescence is specific for each lanthanide ion (due to characteristic 4f energy levels of each ion), presents narrow-emission lines, and weakly depends on the crystalline environment of the host material.

2.1. Understanding temperature quenching of lanthanide luminescence

To understand the effects of temperature on the luminescence of lanthanides, one should first consider the processes which follow the excitation of the electronic states of a substance. The energy of an electronically excited state is lost by a combination of radiative and nonradiative processes. The intensity of the emission, I , is proportional to the population density of electrons in the excited states, $I \propto N$, the temporal evolution of which is described by:

$$\frac{dN}{dt} = -(k_R + k_{NR}) \cdot N(t), \quad (1)$$

where k_R and k_{NR} are the rates of radiative and nonradiative transitions, respectively. Photon emission is created through radiative de-excitation pathways, while nonradiative ones are accompanied by the release of vibrational energy. As a consequence, the electron population in the excited state and the luminescence intensity exponentially decay with a time constant, τ , which is commonly termed the 'lifetime' of the excited state:

$$\tau = \frac{1}{k_R + k_{NR}}. \quad (2)$$

The inverse value of the radiative transition rate is called the 'radiative lifetime' or 'natural lifetime':

$$\tau_R = \frac{1}{k_R}, \quad (3)$$

and can be calculated, in many instances rather well, from the absorption and emission spectra [30, 31] and also from the ratio of the measured lifetime and the quantum efficiency of emission, η :

$$\tau_R = \frac{\tau}{\eta}, \quad (4)$$

the latter of which is defined as the fraction of electrons that underwent radiative decay over the total number of de-excited electrons:

$$\eta = \frac{k_R}{k_R + k_{NR}}. \quad (5)$$

One should note that radiative lifetime values calculated from equation (4) and those obtained from spectroscopy measurements differ in many cases [30]. However, in view of the topic discussed, the more important thing is that radiative lifetime can be considered as temperature-independent for most elaborations.

The intensity of luminescence can be decreased by different processes and such decreases are termed 'quenching'. When quenching occurs due to an increase in the temperature of the material, it is referred as the temperature quenching of luminescence, and it is the underlying phenomena of all luminescence thermometry measurement principles. The temperature dependence of the luminescence emission intensity results from the temperature dependence of the non-radiative transition rate:

$$I(T) = C \cdot k_R \cdot \tau(T) = C \cdot \eta(T) = C \cdot \frac{k_R}{k_R + k_{NR}(T)}, \quad (6)$$

where C is a constant comprised of a number of physical parameters that are characteristic for the measuring system and investigated material (such as the intensity of excitation, the detection geometry, concentration of luminescent species in material and their absorption coefficient and so on) and, in principle, does not change with the temperature.

Therefore, theoretical explanations of temperature-quenching effects are, in fact, related to the description of the temperature-induced changes in the non-radiative transition rate for the material of interest. This description is usually given by a Mott–Seitz theory which is created on a simple configuration coordinate model that consists of two parabolas shifted with respect to each other [32], figure 1. These parabolas represent potential curves, each of which stands for the total energy of the system in its ground or excited state as a function of the configurational coordinate, R .

According to this model, an electron in the excited state, assisted by thermal energy, nonradiatively de-excites to the ground state through the parabola intersection S with the temperature-dependent rate [33]

$$k_{NR}(T) = A \cdot \exp(-\Delta E/k_B T), \quad (7)$$

where ΔE is the energy difference between the lowest level of the excited state and the intersection point of parabolas S , k_B is a Boltzmann constant, and A is a frequency constant (in fact, a quantity only weakly dependent on temperature) of the order of 10¹³ s⁻¹. The nonradiative transition rate is lower for the larger ΔE , and increases with the temperature increase. Expressions for the temperature dependence of luminescence emission intensity and lifetime can be derived by combining equations (6) and (7):

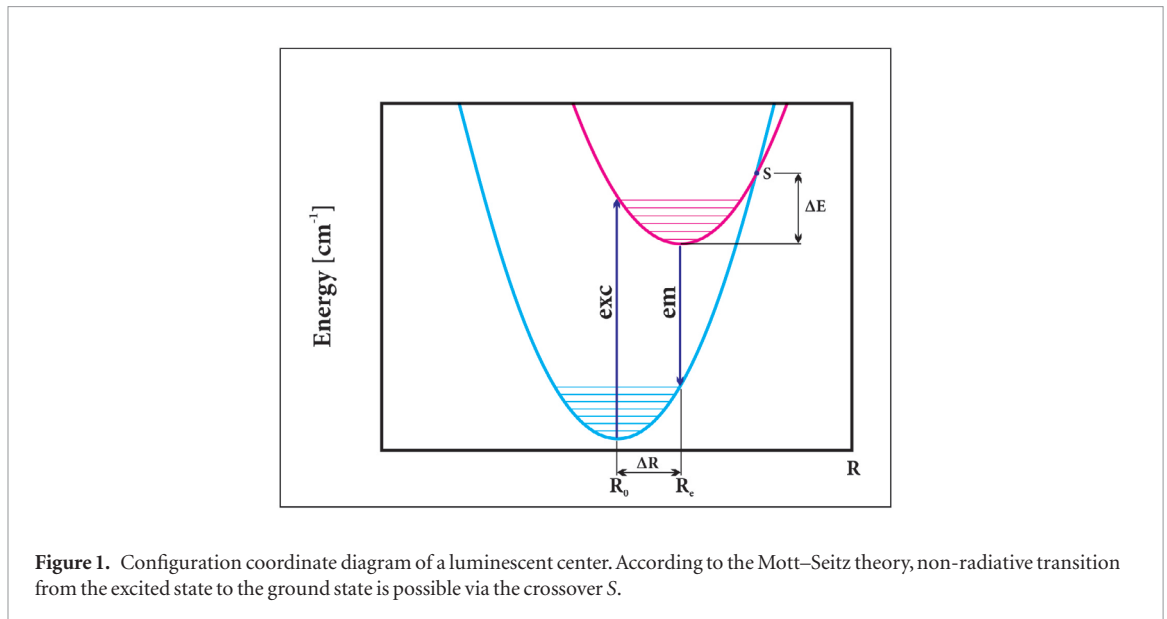


Figure 1. Configuration coordinate diagram of a luminescent center. According to the Mott–Seitz theory, non-radiative transition from the excited state to the ground state is possible via the crossover S.

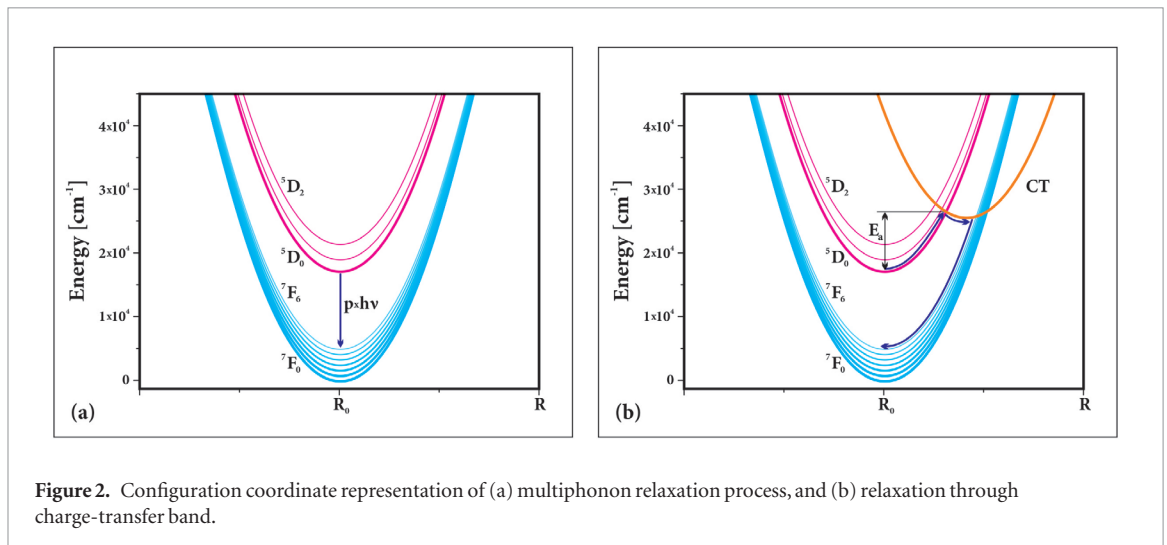


Figure 2. Configuration coordinate representation of (a) multiphonon relaxation process, and (b) relaxation through charge-transfer band.

$$I(T) = C \cdot \frac{1}{1 + \frac{A}{k_R} \cdot \exp(-\Delta E/k_B T)},$$

$$\tau(T) = \frac{1}{k_R + A \cdot \exp(-\Delta E/k_B T)}. \quad (8)$$

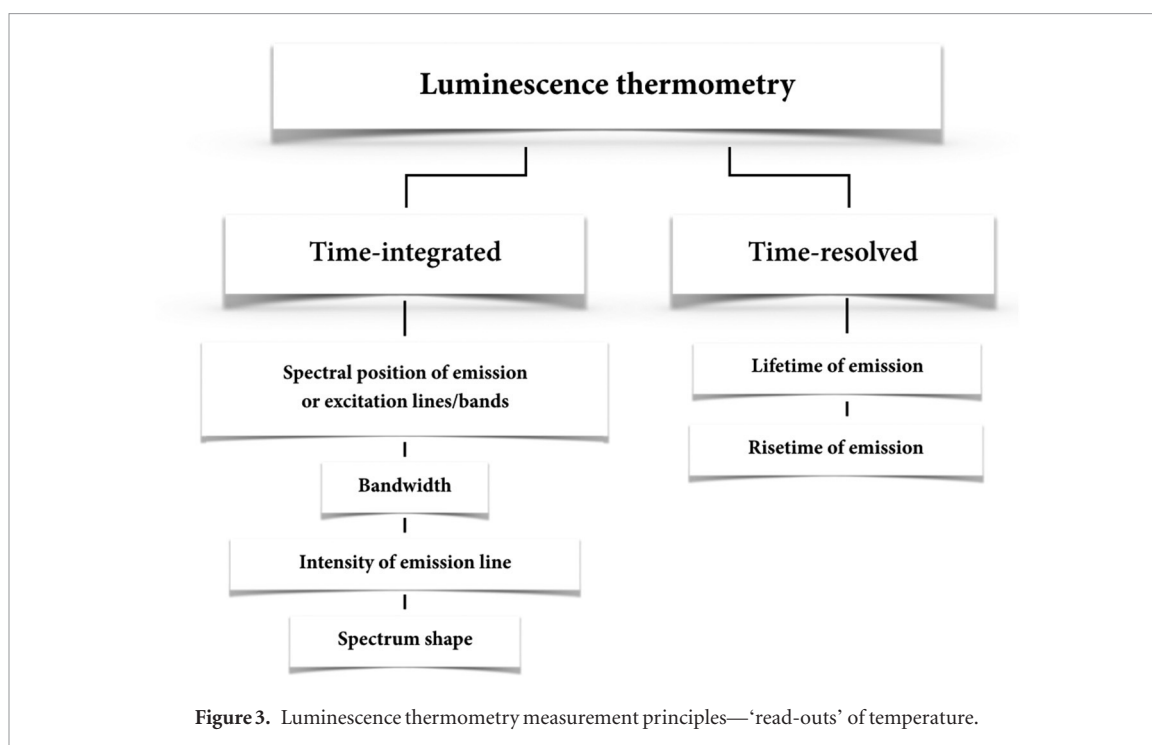
However, the Mott–Seitz theory is more suitable for the explanation of the quenching of broadband emissions (with a large ΔR , see figure 1) than for the quenching of narrow-line f–f emissions that are observed for Ln^{3+} ions (with $\Delta R \approx 0$). Such cases were explained in early works [34–36] by phonon emission to the lattice mode, so-called multiphonon relaxation, schematically depicted in figure 2(a), and described by the following formula:

$$k_{\text{NR}}(T) = k_{\text{NR}}(0) \cdot \left[\frac{\exp(h\nu/k_B T)}{\exp(h\nu/k_B T) - 1} \right]^{\frac{\Delta E}{h\nu}}, \quad (9)$$

where ΔE is the energy difference from the excited level to the next lowest level, $h\nu$ is the dominant phonon energy of the lattice, and $k_{\text{NR}}(0)$ is the value of the nonradiative transition rate at zero temperature which

depends on the electron–lattice coupling strength. The $\Delta E/h\nu$ value actually represents the number of effective phonons that need to be emitted to bridge the energy-gap difference. However, the higher the number of phonons the lower the probability of the process is; it is believed that processes involving more than seven effective phonons are fairly probable. In the case of Eu^{3+} -doped GdVO_4 [37], the multiphonon relaxation process, schematically illustrated in figure 2(a), would require at least 14 phonons of maximal energy (of 885 cm^{-1} [38]) to bridge the gap between $^5\text{D}_0$ and $^7\text{F}_6$ levels ($\sim 12500 \text{ cm}^{-1}$).

Blasse reported the first observation of the role of the charge-transfer state in the temperature quenching of Eu^{3+} luminescence [39]. This nonradiative de-excitation pathway is illustrated in figure 2(b). The minimum of the CT state potential curve has an offset in the configurational coordinate to both excited and ground-state potential curves of Eu^{3+} , therefore, making crossing with them, and thus creating a path for electrons in the excited state to nonradiatively reach the ground state [40, 41]. The rate equation for this process is given by [42]:



$$k_{\text{NR}}(T) = \frac{k_{\text{NR}}(0)}{T^{*1/2}} \cdot \exp(-E_a/k_B T^*),$$

$$T^* = \frac{h\nu}{2k_B} \cdot \coth(h\nu/2k_B T), \quad (10)$$

where E_a is the activation energy of the process.

2.2. Luminescence thermometry measurement principles

Changes in the luminescence of a substance caused by temperature are manifested by several phenomena. Almost all of them may serve as the basis of a temperature measurement, i.e. as the principles of temperature measurement, from which a large number of measurement methods have been derived so far. Depending on the temporal nature of these manifestations, luminescence thermometry measurement principles can be classified as either time-integrated (steady-state) or time-resolved ones. Measurement methods derived from the former principle are implemented with a constant illumination and observation, while those resulting from the latter one are performed with a pulsed or harmonically modulated excitation. Figure 3 illustrates the phenomena that are most commonly used for the development of thermometry methods from the luminescence of lanthanide-ion-doped materials. Some other, quite useful, phenomena are also of importance, such as polarization/anisotropy, but they cannot be implemented using metal oxides and salts.

2.2.1. Changes of energy of emission and excitation lines with temperature

In general, the spectral positions of emission and excitation lines are temperature-dependent in any material. These dependences arise from a number

of processes, such as the changes in the energy of electronic levels, dilatations of the crystal lattice, changes in the refractive index and others. Therefore, measurement procedures can be developed to determine temperature from the luminescence line-shifts, provided that these shifts are sufficiently large to facilitate accurate measurements. However, quite frequently, this condition cannot be fulfilled, especially with the luminescence of lanthanide ions which are fairly dependent on changes in the crystal field acting upon ions ($<0.1 \text{ cm}^{-1} \text{ K}^{-1}$). For example, Kusama *et al* [43] have shown the line-shift of $\text{Y}_2\text{O}_2\text{S}:\text{Eu}^{3+}$ emission ($^5\text{D}_0 \rightarrow ^7\text{F}_0$) from 583.00 to 582.75 nm over the $-16 \text{ }^\circ\text{C}$ to $72 \text{ }^\circ\text{C}$ temperature range (figure 4(a)). Recently, Rocha *et al* [44] have demonstrated that the 863 nm peak in $\text{LaF}_3:\text{Nd}^{3+}$ shifts to longer wavelengths with a temperature increase at an almost constant rate of 0.007 nm K^{-1} (which corresponds to $0.095 \text{ cm}^{-1} \text{ K}^{-1}$ at 863 nm). The development of high-resolution state-of-the-art instruments in recent years may improve conditions of measurement methods based on the line-shifts and expedite their use.

2.2.2. Changes in the emission linewidth with temperature

The density of phonons grows with the increase in temperature of a material. For this reason, emission lines are broadened. In most cases, linewidth linearly depends on temperature. Peng *et al* [45] have shown with $\text{Y}_2\text{O}_3:\text{Eu}^{3+}$ micro- and nanoparticles that the linewidth of $^5\text{D}_0 \rightarrow ^7\text{F}_2$ transition linearly changes for temperatures higher than 70 K. The overall change is about 50 cm^{-1} over the 70–700 K temperature range (figure 4(b)). Recently, Wang *et al* [46] have reported the temperature change in effective linewidths $\Delta\lambda_{\text{eff}}$ ($\Delta\lambda_{\text{eff}} = \int I(\lambda)d\lambda/I_{\text{max}}$; I_{max} is the emission intensity

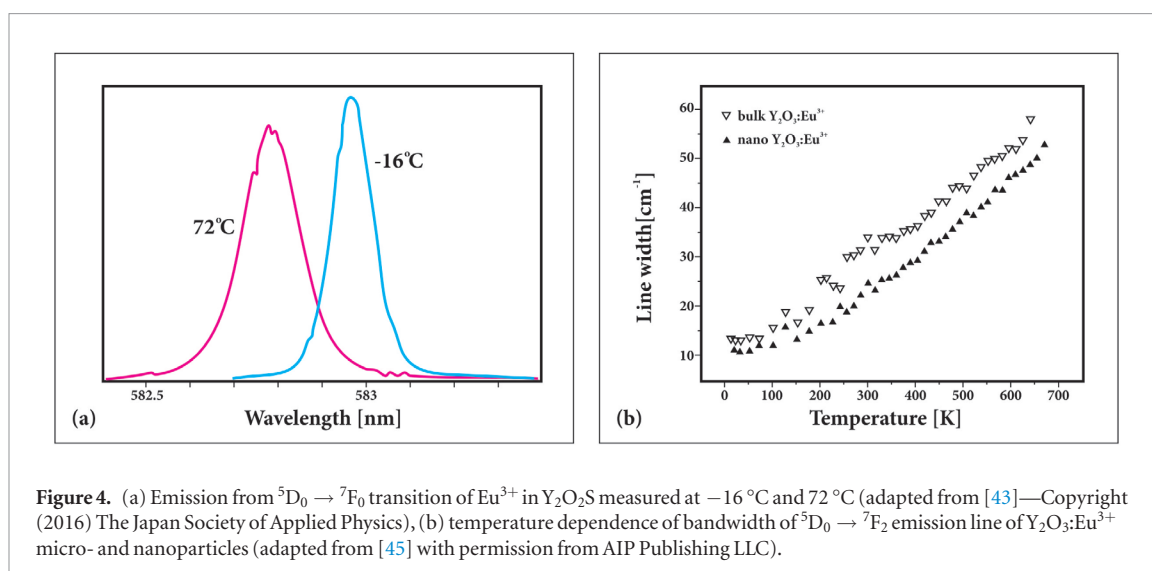


Figure 4. (a) Emission from ${}^5D_0 \rightarrow {}^7F_0$ transition of Eu^{3+} in $\text{Y}_2\text{O}_2\text{S}$ measured at -16°C and 72°C (adapted from [43]—Copyright (2016) The Japan Society of Applied Physics), (b) temperature dependence of bandwidth of ${}^5D_0 \rightarrow {}^7F_2$ emission line of $\text{Y}_2\text{O}_3:\text{Eu}^{3+}$ micro- and nanoparticles (adapted from [45] with permission from AIP Publishing LLC).

at peak emission wavelength) of anti-Stokes emissions in $\text{NaYbF}_4:\text{Tm}^{3+}@\text{SiO}_2$ core-shell microparticles. As the temperature increased from 100 to 700 K, the values $\Delta\lambda_{\text{eff}}$ for the 697 nm and 798 nm emissions non-homogeneously increased from 16.76 nm to 22.94 nm and from 19.79 nm to 25.35 nm, respectively.

2.2.3. Changes in the intensity of the emission line with temperature

As shown in the previous section, the intensity of the emission of lanthanide ions is reduced mainly because of the increase of the non-radiative transition rate with temperature. However, other temperature-dependent mechanisms may also be involved, such as energy transfers between ions, between ions and other quenching centers and to the host and charge-transfer states [47]. In addition, absorption of the host material, the volume of its unit cell and the refraction index may all change with temperature which affects the intensity of the emission line. The major problem in using a single emission line for temperature measurements is that the observed intensity is greatly influenced by changes in measurement conditions. Instabilities in light sources and detectors, if not properly compensated, are the main cause of large measurement errors. Hence, this read-out scheme is almost completely abandoned in current luminescence thermometry applications.

2.2.4. Using the spectrum shape for temperature measurements

Lanthanide-ion-doped materials have rather complex spectra. Emissions may come from more than one excited state, transition may end at different energy levels, and all of them are split into Stark sublevels by crystal field. In addition, materials may present emissions from more than one dopant ion, intrinsic emission of the host material or emission from defect states of the host material, the last of which is particularly important for nanosized materials. Such a complexity of emission spectra provides several excellent opportunities for temperature sensing. The ratio of intensities of different

emission lines is of the utmost importance and probably the most frequently used temperature read-out scheme in luminescence thermometry. It is a self-referencing scheme and eliminates problems caused by changes in measurement conditions. The *radiometric intensity methods* can be classified as those that exploit emissions from (i) a single emission center, and (ii) two or more emission centers. The former are based on the ratio of intensities of emissions that originate from two closely separated excited states of lanthanide ions and, quite rarely, on the ratio of intensity of emission originating from electron transitions that end at different Stark sublevels. The latter method uses the ratio of intensities of emissions from two or more lanthanide ions doped into one host material, or the ratio between the emission of a lanthanide ion and the emission of defect states of the host material. In some cases these methods may be combined to achieve good measurement sensitivity over the wide temperature range, as shown by Čulubrk *et al* [48]. Also, temperature can be extracted from the ratio of intensities of emissions that originate from both thermally coupled and non-coupled excited levels, as demonstrated with $\text{Y}_2\text{O}_3:\text{Er}^{3+}, \text{Yb}^{3+}$ nanopowders by Nikolić *et al* [49]. Recently, neural-network recognition has been used to extract the sample temperature from the shape of emission spectra by Liu *et al* [50]. Even though rhodamine B in a mixture of CuCl_2 and glycerol was used as a temperature probe, this measurement method may also be promising for use with lanthanide luminescence. Up to now, temperature read-out from the ratio of emission intensities that originate from two closely separated excited states of a single lanthanide ion was the most commonly used among all intensity-based methods. However, the relative sensitivity of this method is limited by the value of the energy difference between excited states responsible for the emissions, which will be explained in more detail later in the text. Therefore, the current research is directed toward the development of the radiometric intensity methods which utilize emissions from two or more emission centers in the material.

2.2.5. Temperature measurements from the temporal dependence of emission

The intensity of emission and the lifetime of the excited state from which that emission originates are in a linear relationship (see equation (6)). It seems then that it is equivalent to measure temperature dependence of these quantities. Yet, significant differences exist between these two measurements from the practical point of the realization of luminescence thermometry. In contrast to the temperature read-out from the intensity of a single emission line, the determination of temperature from the emission lifetime is not really compromised by changes in measurement conditions. Additionally, it is not affected by the inhomogeneity of the probe material. Lifetime measurements have better detection limits than intensity ones, which is important for high-temperature applications and, generally, they present smaller uncertainties compared to those in measurements of intensity [7]. They are a self-referencing, like ratiometric intensity methods, but in contrast to them need the observation of just one emission line. The drawback is that lifetime measurements require relatively expensive equipment and, compared to intensity reads, lengthy processing of emission decay data to derive lifetime values. In addition, the temperature change of the excited-state lifetime of lanthanide ions generally shows two regimes. At lower temperatures the change is negligible or relatively small. A sharp decrease in lifetime values occurs at high temperatures. The temperature ranges of these regions are specific for each combination of dopant ion and host material. However, almost constant values of lifetimes are frequently observed around room temperature or in the physiologically important temperature range, limiting the applicability of the method. The problem may be overcome by measuring the rise time of the emission with lanthanide-doped materials of specific characteristics. The rise of an emission occurs in the initial period after the excitation pulse, prior to emission decay, and their values are notably smaller than the lifetime values. They are strongly reduced with temperature increase over the whole dynamic range. One should note that rise times are measured along with lifetimes, i.e. during the same measurement procedure; therefore, it is possible to combine two temperature read-outs in one measurement procedure.

2.3. Figures of merit of luminescence thermometry

The great and ever-increasing number of reports on luminescence thermometry measuring systems, materials and applications necessitates reliable ways of comparing their performance and characteristics. Estimating and reporting the figures of merit of devices and measurement uncertainties in a standardized metrological format is crucial in disseminating results, comparison with theoretical models and competing results. It also increases the public's

confidence in results. One should note that there is no essential difference in the elementary principles of measurement in physics, engineering, chemistry, biology, food science, or luminescence thermometry. Thus, the aforementioned estimating in luminescence thermometry, like in any other field, must be done following universal guidelines for the evaluation of measurement data [51] and reported in wording which is carefully defined in metrology. Because of the importance of terminology and its use in this review, some of the terms will be defined at this point. The definitions are mostly derived from the international vocabulary of metrology (VIM) [52] and assume temperature as the *measurand*—the quantity intended to be measured.

In luminescence thermometry measuring systems do not provide the value of temperature directly; instead they provide the *indication* (Q), which can be, for example, the value of the emission lifetime, the value of the emission intensity or the wavelength of the emission line. The measurement result, i.e. the temperature value, is obtained from a *measurement model*, that is, from the mathematical relation between the temperature, indication and other quantities involved in a measurement. The measurement model is also used to calculate an *uncertainty* in a value of temperature as an estimate of the dispersion of values within which the true temperature value is expected to lie. The uncertainties stem from random variations in replicated independent measurements (so-called type A uncertainties) and systematic effects in the measurement process (so-called type B uncertainties). Type A uncertainties are mostly calculated as a standard deviation of the mean of the measured temperature values. *Accuracy of measurement* is the closeness of agreement between the measured value of temperature and the true value. Accuracy is not a quantity and does not have a numerical value: it is a descriptive parameter. For instance, one can say that measurement is more accurate if it presents a smaller *measurement error*—the measured temperature value minus the reference temperature value. On the other hand, *measurement precision* is a quantity that is expressed numerically by measures of imprecision, usually with a standard deviation or variance. *Precision* is always estimated for a specified *condition of measurement*, such as reproducibility or repeatability conditions, as the closeness of agreement between indications or measured temperature values acquired by replicate measurements on the same objects. Accordingly, *repeatability* is the precision of measurement achieved by replicate measurements over a short period of time under a *repeatability measurement condition* that comprises the same measurement procedure, measuring system, operator, operating conditions and location. Similarly, *reproducibility* is the precision of measurement under a *reproducibility measurement condition* that includes repeated measurements at distinct locations, using different measuring systems

and operators. The most frequently reported figures of merit in the literature on luminescence thermometry are the sensitivity and temperature resolution. The **sensitivity** (S) of a luminescence thermometry measuring system is defined as a quotient of the change in an indication and the change in the temperature value and it is expressed in (unit of indication/K):

$$S = \left| \frac{\partial Q}{\partial T} \right|. \quad (11)$$

Generally, sensitivity depends on the value of the quantity being measured, so it is not particularly suitable for the comparison of results obtained with different measuring systems. For example, let us assume a value of an intensity of emission as an indication. Even with the same measuring system, the indication may be different if measured with different detection amplification gains or with different intensity of excitation. Consequently, the change in the indication with temperature, i.e. the sensitivity, will be different. Frequently, sensitivity is called **absolute sensitivity** to distinguish it from the term **relative sensitivity**, which is defined as the ratio of sensitivity and indication:

$$S_R = \left| \frac{1}{Q} \frac{\partial Q}{\partial T} \right|. \quad (12)$$

Relative sensitivity is, in fact, the normalized value of sensitivity with respect to the indication; it is expressed in K^{-1} and is suitable for the comparison of results. Sometimes, relative sensitivity is multiplied by 100 and presented as a percentage change in the indication value per unit change in the temperature, $\%K^{-1}$. **Temperature resolution** (ΔT_{\min}) is the smallest change in a temperature that causes a perceptible change in the indication; it is presented in kelvins and is calculated as the ratio of uncertainty (expressed by the standard deviation, σ) and sensitivity [47]:

$$\Delta T_{\min} = \frac{\sigma}{S}. \quad (13)$$

Temperature resolution strongly depends on the characteristics of a measuring system (for example, on the noise), but it also depends on the indication value. The **spatial resolution** of a measuring system is defined as the minimum distance between points of a measurement (Δx_{\min}) that can be resolved under a temperature resolution of the system [53], and can be calculated as [54]:

$$\Delta x_{\min} = \frac{\Delta T_{\min}}{\left| \frac{dT}{dx} \right|}. \quad (14)$$

However, the spatial resolution is restricted by the Rayleigh diffraction limit, which can be calculated from the maximal wavelength of the emission used in the measuring system and its numerical aperture. The ability of a luminescence temperature measuring system to follow temporal changes in temperature is presented by its **temporal resolution** (Δt_{\min}) which is defined as the minimum period of time between

measurements capable of resolving a temperature higher than the temperature resolution [53]:

$$\Delta t_{\min} = \frac{\Delta T_{\min}}{\left| \frac{dT}{dt} \right|}. \quad (15)$$

3. Temperature sensing from spectral features of lanthanide-downshifting emission

Among different read-outs of temperature from spectral features of luminescence, temperature evaluation by relative emission-intensity measurements (ratiometric intensity measurements) are of particular importance and prevalently used with lanthanide-doped metal oxides and salts. This is because ratiometric measurements alleviate problems occurring with fluctuations in excitation and electronic drifts in detection and, more importantly, because ratiometric methods are self-referencing, i.e. measurements do not have to refer to any temperature standard. Ratiometric read-outs of temperature can be successfully realized with any combination of lanthanide emissions, whether they come from single or multiple emission centers, providing that temperature dependences of these emissions have distinct behaviors.

3.1. The ratiometric method utilizing emissions from closely separated excited levels of trivalent lanthanide ions

The luminescence intensity ratio (LIR) of emissions from closely separated excited levels is by far the most utilized read-out of temperature in methods employing lanthanide ions. Two excited energy states of lanthanide ions are thermally coupled when they are separated by an energy difference of $\sim 2000 \text{ cm}^{-1}$ or less, which means that they are separated by an energy gap sufficiently small to permit the promotion of electrons to the higher energy state from a lower one using thermal energy [47]. In this case, both states share the electronic population according to Boltzmann's distribution,

$$N_H = N_L \cdot \exp(-\Delta E/k_B T), \quad (16)$$

where N_H and N_L are the number of electrons in the higher and lower excited state, respectively, ΔE is the energy difference between these states, k_B is Boltzmann's constant, and T is absolute temperature. Then, the LIR of emissions from higher (I_H) and lower (I_L) excited states can be approximated as follows [21]:

$$\text{LIR}(T) = \frac{I_H(T)}{I_L(T)} = C \cdot \frac{g_H A_H h \nu_H}{g_L A_L h \nu_L} \cdot \exp(-\Delta E/k_B T) = B \cdot \exp(-\Delta E/k_B T), \quad (17)$$

where h is Planck's constant, g is the degeneracy of the excited state, A is the spontaneous emission rate, ν is the emission frequency, while H and L denote 'higher' and

'lower' energy states. At low temperatures the higher energy state will not be populated because electrons do not have enough thermal energy to bridge the energy gap, and because the non-radiative relaxation rate from the higher to lower energy state is very large for the closely spaced states. Therefore, the LIR read-out scheme has a low-temperature bound that is proportional to ΔE , so that the smaller the ΔE , the lower the temperature from which LIR can be used. As temperature increases, the higher energy state becomes populated, and hence the emission from this state gradually increases in intensity, at the expense of the population of the lower state. However, both emissions lessen in intensity because of temperature quenching (as described in the section 2.1) until one of them, or both, become undetectable. The upper temperature bound of LIR applicability thus depends mainly on the phonon spectrum of the host material and the type of lanthanide ion involved. One should note that measurement uncertainties become higher near these limits. One should also note that with the LIR method it is possible to use any emissions providing that they originate from two thermally coupled excited levels. For example, it is possible to use any combination of emissions from ${}^5D_1 \rightarrow {}^7F_J$ and ${}^5D_0 \rightarrow {}^7F_J$ transitions of Eu^{3+} ion.

For the assessment of the material performance in the LIR technique, experimental data are fitted to the theoretical equation (17) to obtain B and ΔE . However, the natural logarithm of equation (17) shows that $\log(\text{LIR})$ has a linear dependence on inverse temperature:

$$\log(\text{LIR}) = \log(B) - \frac{\Delta E}{k_B} \cdot \frac{1}{T}. \quad (18)$$

The values of $\Delta E/k_B$ and $\log(B)$ can be easily found as the line-slope and intercept with y -axes of the $\log(\text{LIR})$ versus $1/T$ linear fit, respectively. Expressions for the absolute and relative sensitivities of LIR measurements can be derived from equations (11), (12) and (17):

$$S(T) = \frac{\Delta E}{k_B T^2} \cdot B \cdot \exp(-\Delta E/k_B T) = \frac{\Delta E}{k_B T^2} \cdot \text{LIR}(T),$$

$$S_R(T) = \frac{\Delta E}{k_B T^2} \cdot 100\%. \quad (19)$$

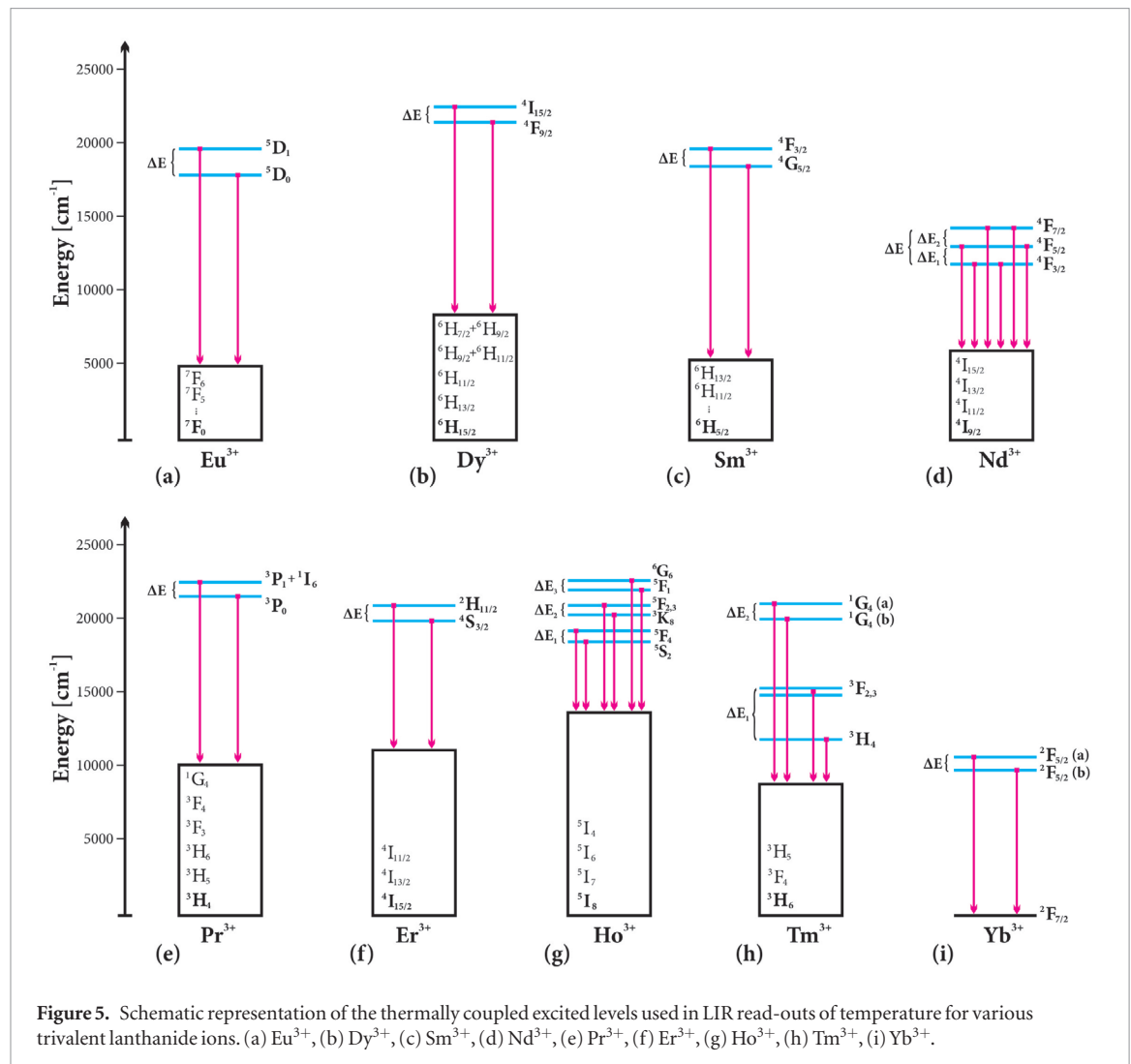
It should be noted that both sensitivities are functions of temperature; when reporting their values it is important to state for which temperature they were calculated. For example, for any material the value of relative sensitivity at 300 K reduces by 20% at 335 K, by 50% at 424 K and by 90% at 950 K (if still in a measurement range). The relative sensitivity crucially depends on the type of lanthanide ion used, that is, on the energy difference between its thermally coupled excited states; the larger the ΔE the higher value of relative sensitivity. The value of ΔE of a particular ion just slightly varies between different hosts (max. up to few hundreds cm^{-1}). Therefore, relative sensitivities of LIR using particular lanthanide ions will be pretty

Table 1. Summary of thermally coupled energy levels of different trivalent lanthanide ions that are commonly exploited by LIR technique, emission colors, usual energy difference between coupled levels (ΔE), and theoretical relative sensitivity at 300 K. a: low energy Stark component, b: high energy Stark component.

Ion	Coupled excited levels		Emission color	ΔE (cm^{-1})	Relative sensitivity at 300 K ($\%K^{-1}$)
	High	Low			
Eu^{3+}	5D_1	5D_0	Green/red	1750	2.80
Dy^{3+}	${}^4I_{15/2}$	${}^4F_{9/2}$	Blue	1000	1.60
Sm^{3+}	${}^4F_{3/2}$	${}^4G_{5/2}$	Green/orange/red	1000	1.60
Nd^{3+}	${}^4F_{5/2}$	${}^4F_{3/2}$	NIR	1000	1.60
Nd^{3+}	${}^4F_{3/2}$ ^b	${}^4F_{3/2}$ ^a	NIR	100	0.16
Pr^{3+}	3P_1	3P_0	Green or red	580	0.93
Er^{3+}	${}^2H_{11/2}$	${}^4S_{3/2}$	Green	780	1.25
Ho^{3+}	5F_4	5S_2	Green	120	0.19
Tm^{3+}	${}^3F_{2,3}$	3H_4	Red/NIR	1700	2.72
Tm^{3+}	1G_4 ^b	1G_4 ^a	Blue	100	0.16
Yb^{3+}	${}^2F_{5/2}$ ^b	${}^2F_{5/2}$ ^a	NIR	680	1.09

much the same irrespective of the host material. The thermally coupled energy levels of different trivalent lanthanide ions that are commonly exploited by LIR technique are given in table 1 and schematically presented in figure 5.

The thermally coupled excited levels of Eu^{3+} ions ($4f^6$ electron configuration) whose emissions are utilized for LIR are 5D_1 and 5D_0 , which are separated by approximately 1750 cm^{-1} , figure 5(a). This is, in fact, the largest energy gap among all trivalent lanthanide ions used for LIR thermometry and, therefore, LIR thermometry with Eu^{3+} has the worst low-temperature boundary, but the highest relative sensitivity. In the case of Dy^{3+} ions ($4f^9$ electronic configuration) LIR uses emissions from the ${}^4I_{15/2}$ and ${}^4F_{9/2}$ adjacent excited levels (figure 5(b)), and for Sm^{3+} ($4f^5$ electronic configuration) emissions from the ${}^4F_{3/2}$ and ${}^4G_{5/2}$ levels are used (figure 5(c)). In both cases, the energy difference between the levels is approximately 1000 cm^{-1} . The energy levels of interest for Nd^{3+} ($4f^3$ electronic configuration) are the ${}^4F_{7/2}$, ${}^4F_{5/2}$ and ${}^4F_{3/2}$, figure 5(d). The emissions from the ${}^4F_{5/2}$ and ${}^4F_{3/2}$ levels are commonly used for LIR (the energy difference is 1000 cm^{-1}). In addition, the ratios of emissions from the ${}^4F_{3/2}$ Stark sub-levels are also utilized, but with low relative sensitivity because of the small energy gap between the sub-levels (of the order of 100 cm^{-1}). In the case of Pr^{3+} ($4f^2$ electronic configuration) the LIR method can use emissions from the ${}^3P_1 + {}^1I_6$ and 3P_0 levels, which are separated by approximately 580 cm^{-1} (figure 5(e)). LIR using Er^{3+} ions ($4f^{11}$ electronic configuration) uses the emissions of the ${}^2H_{11/2}$ and ${}^4S_{3/2}$ levels (an energy gap of approximately 780 cm^{-1}), as shown in figure 5(f). Ho^{3+} ($4f^{10}$ electronic configuration) presents three combinations of thermally coupled levels: ${}^5F_4 - {}^5S_2$, ${}^5F_{2,3} - {}^3K_8$, and ${}^5G_6 - {}^5F_1$ whose emissions can be utilized for LIR thermometry (figure 5(g)). Tm^{3+}



($4f^{12}$ electronic configuration) has two couples of adjacent thermally coupled levels, ${}^3\text{F}_{2,3}$ and ${}^3\text{H}_4$, and ${}^1\text{G}_{4(a)}$ and ${}^1\text{G}_{4(b)}$, whose emission intensity ratios are strongly temperature-dependent (figure 5(h)). In the case of Yb^{3+} ($4f^{13}$ electronic configuration), thermometry can be based on the LIR of the emissions of the ${}^2\text{F}_{5/2}$ Stark sublevels (an energy difference of 680 cm^{-1}), as shown in figure 5(i).

It is important to note that table 2 presents ΔE values obtained by the fitting of experimental LIR temperature dependences to the theoretical model given by equations (17) or (18). Quite frequently, this value deviates from the value obtained spectroscopically (as a difference between respected emission barycenters— ΔE_S) or from the value obtained by theoretical elaborations. The difference can be quantified through the error parameter $\delta = |\Delta E - \Delta E_S| / \Delta E_S$ [23]. A large value of δ implies either an error in the measurement and fitting procedure, or that some other mechanism apart from Boltzmann's re-distribution of the population takes place in materials as the temperature increases. Such mechanisms may be, for example, energy transfers between thermally coupled levels, other levels or charge-transfer bands.

3.2. Ratiometric methods that exploit emissions from multiple emission centers in one host

The LIR read-out of temperature is not necessarily limited to the use of emissions from adjacent excited energy levels. It can be used with any combination of emissions that originate from one or more emission centers. An ideal case in terms of a simple theoretical interpretation would be the one where one of the emissions does not change in the temperature range of measurement, $I_R = \text{const}$. Then, LIR temperature dependence could be explained using the theoretical models described in section 2.1, and would also have the same trend as the temperature dependence of the excited-state lifetime [92]. On the basis of equation (6), the following expression can be easily derived:

$$\text{LIR}(T) = \frac{I(T)}{I_R} = C_1 \cdot k_R \cdot \tau(T) = C \cdot \frac{k_R}{k_R + k_{NR}(T)}, \quad (20)$$

where C_1 is a constant that is characteristic for the measuring system and the investigated material. This case can be realized using the emissions of rare earths incorporated into the wide band-gap nanocrystalline host materials whose trap emission can serve as

a reference emission. This concept was originally demonstrated with $\text{Zn}_2\text{SiO}_4:\text{Mn}^{2+}$ using the ratio of the transition-metal ion emission and the trap emission of the host material [93]. Nikolić *et al* [92] and Dramićanin *et al* [94] have demonstrated LIR thermometry in Eu^{3+} -doped and Sm^{3+} -doped anatase TiO_2 nanocrystals, respectively, where the trap emission of TiO_2 [95], with maximal value at 438 nm, was considered temperature-independent and served as a reference. The presence of dopant luminescence centers led to the appearance of energy states within the band gap of TiO_2 , shown in figure 6, whose emissions were strongly quenched by temperature.

By monitoring the LIR of the 613 nm ($\text{Eu}^{3+5}\text{D}_0 \rightarrow {}^7\text{F}_2$ transition) and 438 nm emissions (the trap emission), luminescence thermometry was accomplished over the 307–533 K temperature range with a maximum relative sensitivity of $2.43\% \text{K}^{-1}$ @ 533 K and a temperature resolution of 0.46 K. The ratio of Sm^{3+} emission at 612 nm (${}^4\text{G}_{5/2} \rightarrow {}^6\text{H}_{5/2}$ transition) and the trap emission provided measurements over a slightly smaller temperature range (307–483 K), but with an excellent relative sensitivity of $10.54\% \text{K}^{-1}$ @ 328 K. In addition, in both cases the thermometry using emission-lifetime temperature dependences has been demonstrated over the same temperature intervals. The use of the trap emission as a reference emission has also been demonstrated with Eu^{3+} -doped $\text{Gd}_2\text{Ti}_2\text{O}_7$ nanocrystals [61] (303–423 K range, relative sensitivity from 0.14 to $0.46\% \text{K}^{-1}$) and Dy^{3+} -doped $\text{Gd}_2\text{Ti}_2\text{O}_7$ [48] nanocrystals (293–423 K range, relative sensitivity from 0.133 to $1.127\% \text{K}^{-1}$), along with the conventional LIR of emissions from two excited levels of rare-earth ions. Recently, Das *et al* [96] have implemented the same approach using the ratio of the trap emission of a SrZrO_3 host and the emission of a Eu^{3+} dopant over the 293–423 K range with a maximum relative sensitivity of $2.22\% \text{K}^{-1}$ at 460 K. In addition, the authors have demonstrated temperature read-out from the Eu^{3+} emission decays. It is worth noting that these materials provide two LIR read-out schemes. For example, by combining two LIR approaches it was possible to obtain a relative sensitivity higher than $0.9\% \text{K}^{-1}$ over the complete measurement range [48].

The LIR of arbitrary emissions of $\text{YAG}:\text{Tb}^{3+}$ has been demonstrated over the 293–423 K range [97]; temperature dependence of the 541 nm/547 nm emission ratio was approximated by a polynomial function. The LIR of two emission centers in one host has been demonstrated by Tripathi *et al* [98] for Sm^{3+} (0.25 mol%) and Eu^{3+} (1 mol%) co-doped $\text{CaO-Li}_2\text{O-B}_2\text{O}_3\text{-BaO}$. A similar approach to thermometry has been realized using $\text{Ho}^{3+}\text{-Tm}^{3+}$ co-doped Y_2O_3 [99], but employing up-conversion emission. Ding *et al* [100] have shown that the LIR between the Tb^{3+} (${}^5\text{D}_4 \rightarrow {}^7\text{F}_5$ transition) and Eu^{3+} (${}^5\text{D}_0 \rightarrow {}^7\text{F}_2$ transition) emissions in $\beta\text{-NaYF}_4:\text{Ce}^{3+}, \text{Tb}^{3+}, \text{Eu}^{3+}$ microcrystals is linearly related to the temperature over the 300–573 K range; the observed maximum relative sensitivity is $0.46\% \text{K}^{-1}$.

The LIR between the Tb^{3+} and Eu^{3+} emissions has also been investigated by Marciniak and Bednarkiewicz [101] using $\text{LiLaP}_4\text{O}_{12}:\text{Tb}^{3+}, \text{Eu}^{3+}$ nanocrystals. The thermometers studied could be applied to a 77–600 K range with a relative sensitivity up to $1\% \text{K}^{-1}$. The LIR of emissions from two lanthanide ions, the 1060 nm emission of Nd^{3+} and the 980 nm emission of Yb^{3+} has been demonstrated by Marciniak *et al* [102]. They used core-shell nanoparticles that consisted of an Yb-Er co-doped $\beta\text{-NaYF}_4$ core and an active Yb-Nd co-doped $\beta\text{-NaYF}_4$ shell (figure 7(A)). Thermometry was achieved from the downshifting emission after an ~ 808 nm excitation with $2.1\% \text{K}^{-1}$ relative sensitivity, but also from the ratio of upconversion emissions coming from the $\text{Er}^{3+4}\text{S}_{3/2}$ and ${}^2\text{H}_{11/2}$ levels (figure 7(B)).

Wang *et al* [103] were the first to show the LIR between emissions from transition metal and lanthanide ions co-doped into the same host. $\text{ZnS}:\text{Mn}^{2+}/\text{Eu}^{3+}$ quantum dots showed the 595 nm emission from the $\text{Mn}^{2+4}\text{T}_1 \rightarrow {}^6\text{A}_1$ transition and the 612 and 588 nm emissions from the $\text{Eu}^{3+5}\text{D}_0 \rightarrow {}^7\text{F}_2$ and ${}^5\text{D}_0 \rightarrow {}^7\text{F}_1$ transitions, respectively. The ratio of these intensities yielded a linear relationship over the 303–413 K range. The LIR of transition metal and lanthanide ion NIR (near-infrared) emissions have been recently demonstrated by Marciniak *et al* [104] using $\text{LiLaP}_4\text{O}_{12}:\text{Cr}^{3+}, \text{Nd}^{3+}$ nanocrystals. The wide operating range (113–453 K), high relative sensitivity of $4.89\% \text{K}^{-1}$ at 323 K, and high repeatability (a variance lower than 0.3% between measurements) shows the excellent potential of this method for operating in the NIR range.

Recently, using nano- and microcrystals of $\text{Y}_2\text{O}_3:\text{Eu}^{3+}$, Souza *et al* [105] have reported a new ratiometric read-out of temperature based on the ratio between the emission intensities of the ${}^5\text{D}_0 \rightarrow {}^7\text{F}_4$ transition when the ${}^5\text{D}_0$ emitting level is excited through the ${}^7\text{F}_2$ or ${}^7\text{F}_1$ level. They were able to measure temperatures between 180 and 323 K with a relative sensitivity ranging from 0.7 to $1.7\% \text{K}^{-1}$. With this approach the calibration factor can be calculated from the Eu^{3+} emission spectrum, avoiding the need for new calibration procedures whenever the thermometer operates in different media.

4. Temperature sensing from changes in the temporal behavior of lanthanide emission

Generally, time-integrated measurements are simpler than time-resolved ones since they require less complex instrumentation, and they are also more regularly practiced these days. However, being simply an average of the time-resolved phenomena, time-integrated measurements do not account for all the information imparted by luminescence. It should be noted that all the aforementioned methods can also be realized through a pulsed excitation and, under certain conditions, with delayed detection. In fact,

Table 2. A summary of metal oxides and salts used in thermometry based on the LIR of downshifting emissions from closely separated excited levels of lanthanides along with data on their shape, method of preparation, working temperature range, relative (S_R) and absolute sensitivity (S), as well as the energy difference between coupled levels (ΔE) given according to literature reports.

Ion	Material	Shape	Synthesis	Range (K)	S_R (%K ⁻¹)	S (K ⁻¹)	ΔE (cm ⁻¹)	Ref.
Eu ³⁺	LiNbO ₃	C	Czochralski	303–723		0.0007	2720	[55]
Eu ³⁺	Gd ₂ O ₃	P	Combustion	300–800		0.0007@800 K	1500	[56]
Eu ³⁺	NaEuF ₄	P	Hydrothermal	298–523	0.43@293 K		1690	[57]
Eu ³⁺	Lu ₂ O ₃	NC	PCS	293–823		0.0004@823 K	1596	[58]
Eu ³⁺	GdAlO ₃	P	Solid-state	293–773	2.96@293 K		1745	[59]
Eu ³⁺	CaEu ₂ (WO ₄) ₄	P	Solid-state	300–500		0.014@300 K	1068	[60]
Eu ³⁺	Gd ₂ Ti ₂ O ₇	NC	PCS	303–423	0.95@423 K	0.015@423	1718	[61]
Eu ³⁺	YNbO ₄	P	Solid-state	303–803		0.0035@700 K	1617	[62]
Eu ³⁺	(Y _{0.75} Gd _{0.25}) ₂ O ₃	NC	PCS	293–773		0.0049@823	1633	[63]
Eu ³⁺	Tellurite	G	MQ	293–480	2.75@300 K		1725	[64]
Eu ³⁺	Calibo	G	MQ	293–550	2.75@300 K		1725	[64]
Eu ³⁺	GdVO ₄	P	Solid-state	298–823		0.0168@298 K	1530	[37]
Dy ³⁺	BaYF ₅	NC	Solvothermal	293–773	1.22@293 K		1047	[65]
Dy ³⁺	BaYF ₅ ^a	NC	Solvothermal	293–693	1.11@293 K		954	[65]
Dy ³⁺	Gd ₂ Ti ₂ O ₇	NC	PCS	293–443	1.68@293 K		1002	[48]
Dy ³⁺	Al ₂ O ₃	P	Combustion	298–723		0.0014	1117	[66]
Dy ³⁺	Y ₃ Al ₅ O ₁₂	NC	Co-precipitation	293–623				[67]
Dy ³⁺	Y ₃ Al ₅ O ₁₂	CT	Paint	300–900				[68]
Dy ³⁺	Y ₃ Al ₅ O ₁₂	P	Commercial	293–1573				[69]
Dy ³⁺	B ³⁺ -N ³⁻ -Y ₃ Al ₅ O ₁₂	P	Sol-gel	500–1500				[70]
Dy ³⁺	Y ₄ Al ₂ O ₉	C	MP	296–1273		0.003@873 K	1000	[71]
Dy ³⁺	GdVO ₄	P	Solid-state	298–678		0.01@336 K	1263	[37]
Dy ³⁺	GdVO ₄	TF	PLD	300–473	2.00@300 K		1270	[72]
Dy ³⁺	LaF ₃	NC	MQ	298–523			1245	[73]
Sm ³⁺	Lu ₂ O ₃	NC	PCS	293–823		0.0004@823 K	1596	[58]
Sm ³⁺	YNbO ₄	P	Solid-state	303–773	0.43@500 K	0.0007@700 K	1455	[74]
Sm ³⁺	GdVO ₄	P	Solid-state	293–823		0.00045@750 K	1038	[75]
Sm ³⁺	Y ₂ O ₂ S	P	Commercial	293–1100			763	[76]
Nd ³⁺	Gd ₂ O ₃	NR	Co-precipitation	288–323	1.75@288 K		1092	[77]
Nd ³⁺	β -NaYF ₄	P	Hydrothermal	323–673	1.12@500 K	0.0082@500 K	1001	[78]
Nd ³⁺	La ₂ O ₂ S	P	Solid-state	30–600	1.58@300 K		987	[79]
Nd ³⁺	La ₂ O ₂ S ^b	P	Solid-state	30–600	0.18@300 K		110	[79]
Nd ³⁺	LaF ₃ ^b	NC	Co-precipitation	298–338	0.1@298 K			[44, 80]
Nd ³⁺	α -NaYF ₄ ^b	NC	TD	273–423	0.12@273 K	0.0098@273 K	60	[81]
Nd ³⁺	LiNdP ₄ O ₁₂ ^b	NC	Co-precipitation	200–500	0.22@313 K		70	[82]
Nd ³⁺	Y ₃ Al ₅ O ₁₂ ^b	NC	Combustion	288–343	0.15@300 K		95	[83]
Nd ³⁺	YVO ₄ ^b	NC	Pechini	298–333	0.19@298 K		90	[84]
Nd ³⁺	YVO ₄ ^c	NC	Pechini	298–333	0.15@298 K		90	[84]
Nd ³⁺	P–K–Ba–Al	G	MQ	300–850	1.5@300 K		957	[85]
Nd ³⁺	Silica	F			1.68@293 K			[86]
Pr ³⁺	(K _{0.5} Na _{0.5})NbO ₃	P	Solid-state	293–456			5558	[87]
Pr ³⁺	β -NaYF ₄	P	Hydrothermal	120–300	0.731@300 K		457	[88]
Pr ³⁺	Lithium tellurite	G	MQ	273–423	0.97@300		607	[89, 90]
Er ³⁺	Yttria-stabilized zirconia	P	Reverse co-precipitation	123–423		0.0015@423	64	[91]

^a Using different emissions for LIR.

^b LIR of emissions for Stark components of ⁴F_{3/2} (transition to ⁴I_{9/2}).

^c LIR of emissions for Stark components of ⁴F_{3/2} (transition to ⁴I_{11/2}).

Abbreviations: *shape*: P—powder, C—crystal, NC—nanocrystal, NR—nanorods, CT—coating, F—fiber, TF—thin film; *synthesis*: MQ—melt-quenching method; PCS—polymerized complex solution method, MP—micro-pulling-down method, TD—thermal decomposition, PLD—pulsed laser deposition).

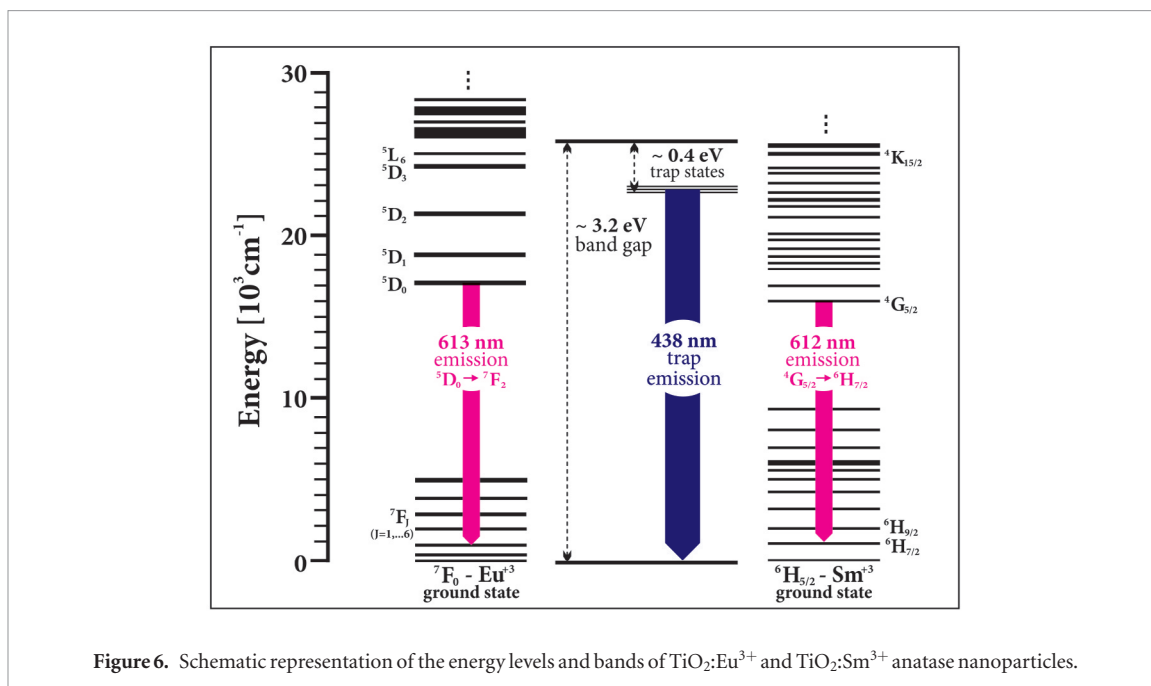


Figure 6. Schematic representation of the energy levels and bands of $\text{TiO}_2:\text{Eu}^{3+}$ and $\text{TiO}_2:\text{Sm}^{3+}$ anatase nanoparticles.

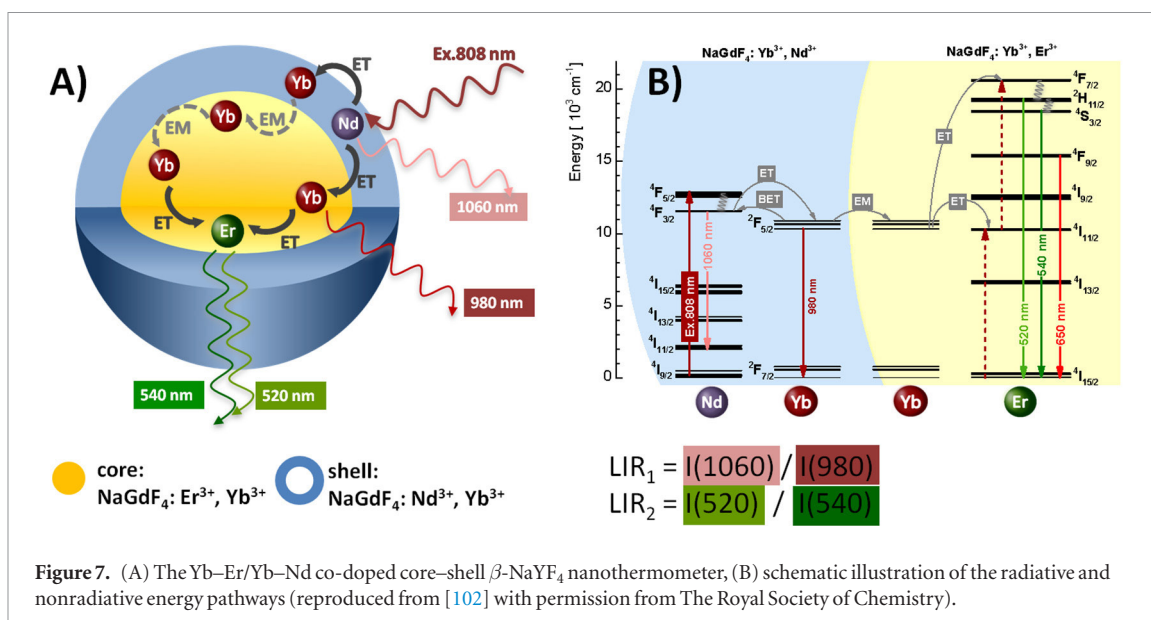


Figure 7. (A) The Yb–Er/Yb–Nd co-doped core–shell $\beta\text{-NaYF}_4$ nanothermometer, (B) schematic illustration of the radiative and nonradiative energy pathways (reproduced from [102] with permission from The Royal Society of Chemistry).

delayed detection can eliminate some problems that compromise time-integrated measurements, such as strong background luminescence, and thus improve measurement accuracy. However, delays in detection should be considerably shorter than the lifetimes of any of the emission involved. Nonetheless, in terms of luminescence thermometry, the time-resolved measurements of interest are the measurements of emission decay times and rise times.

4.1. Decay-time-based sensing of temperature

Time-domain and frequency-domain methods are commonly used for measurements of emission decay times; the first method utilizes pulsed excitation sources while the latter uses intensity-modulated continuous-wave light sources. So far, only a few reports have been published on temperature sensing from the frequency-domain measurements of emission decay times and

none, to the best of my knowledge, which are related to lanthanide luminescence. Reports considering the use of the time-domain method for the read-outs of temperature from decay times, on the other hand, are extensive.

The temperature dependence of the excited-state lifetime, as discussed in section 2.1, results from the temperature dependence of the non-radiative transition rate. Generally, it shows two distinctive behaviors which can be easily understood from equation (2) when rewritten in the following form:

$$\tau(T) = \frac{\tau_R(T)}{1 + \tau_R(T) \cdot k_{NR}(T)}. \quad (21)$$

At low temperatures, where the values of the non-radiative rate are negligible, the lifetime is equal to the radiative lifetime, $\tau \cong \tau_R$. In principle, radiative lifetime only slightly changes with temperature:

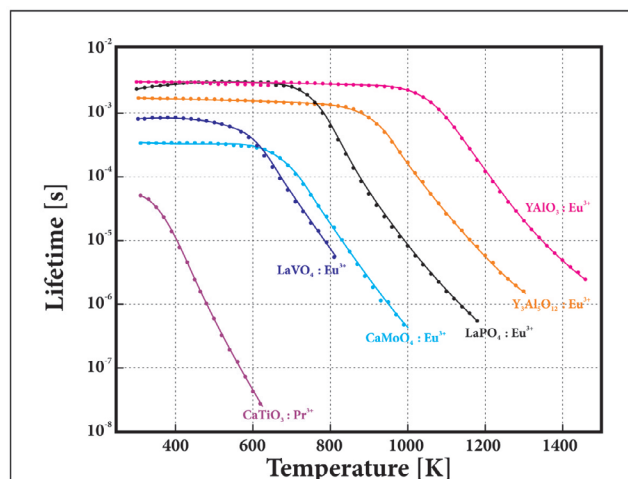


Figure 8. Temperature dependences of emission-lifetime values of some lanthanide-doped metal oxides and salts (adapted from 19 with permission from Elsevier).

$\tau_R(T) = \tau_{R0} \exp(-\alpha \cdot T)$, where α is the phenomenological parameter of order 10^{-4} K^{-1} or less. Therefore, at low temperatures lifetime only slightly decreases with temperature increase or does not change at all. As a consequence, the decay-time method is practically insensitive to temperature changes. This temperature range of insensitive response is followed by one in which lifetime steeply decreases with temperature due to a strong increase in the non-radiative rate (equations (7), (9) and (10)). The temperature point of the transition between two regions essentially depends on the energy difference between lanthanide's excited level and the closest lower energy level or charge-transfer band and on the phonon energy of the host material. Examples of lifetime temperature dependences of some lanthanide-doped metal oxides and salts are given in figure 8. The temperature region of decay-time insensitivity represents the major obstacle to its use. This region frequently covers the physiologically relevant temperature range and thus prevents the use of many probes for decay-time read-out of temperature in biomedicine. On the other hand, in the temperature region of the steep decay-time decrease the method is very sensitive. One should note that the uncertainties in decay times are generally smaller than those in emission intensities and that current technology facilitates measurements of very short decay times. For these reasons, decay-time methods have the potential to present better temperature resolutions than intensity-based measurements and have larger high-temperature operating bounds. An overview of lanthanide-ion-doped metal oxides and salts used for decay-time read-out of temperature is given in table 3.

4.2. Rise-time-based sensing of temperature

The temporal dependence of an emission generally shows three distinct behaviors, as described in figure 9(a). In the first time period, the emission follows (resembles) the time dependence of the excitation pulse.

In the second, the emission intensity rises due to the accumulation of electrons in the excited level, and then, in the third period, the emission decreases due to the processes that were discussed in previous sections. The first two periods are relatively short by comparison with the third, and in routine analyses they are frequently not measured (so-called 'dead time' [129]). However, the initial rise of an emission may be very useful for the determination of temperature. Ranson *et al* [130] were the first to report the temperature dependence of the rise time of the emission from the $^5D_0 \rightarrow ^7F_2$ transition of Eu^{3+} incorporated into Y_2O_3 . They found that the rise time exponentially decreases over the 298–1073 K temperature range; from the reported data it is possible to estimate that the relative sensitivity was $\approx 3\% \text{ K}^{-1}$ @ 298 K and $\approx 0.2\% \text{ K}^{-1}$ @ 1073 K. Later, Allison *et al* [131] measured the emission rise time of the same material (but doped with 0.5 at% of Eu^{3+}). They found a linear decrease in rise-time values from 110 to 9 μs over the 295–973 K temperature range; an absolute sensitivity of $0.15 \mu\text{s} \cdot \text{K}^{-1}$ over the complete temperature range and relative sensitivities of $0.14\% \text{ K}^{-1}$ @ 295 K and $1.66\% \text{ K}^{-1}$ @ 973 K may be estimated from the reported data.

The accumulation of electrons on the 5D_0 excited level of Eu^{3+} ions in the C_2 site of Y_2O_3 occurs at short times after excitation by a fast transition from (i) the higher excited states ($^5D_1, ^5D_2, \dots$), (ii) by energy transfer from neighboring Eu ions situated in C_{3i} sites, and (iii) by energy migration from other Eu ions, as shown in figure 9(b). Then, according to Ranson *et al* [130] the number of electrons in the emitting level, N , can be described as:

$$N = N_0 + N_1 \cdot [1 - \exp(-t/\tau_r)], \quad (22)$$

where N_0 stands for the population directly excited within the ion, N_1 stands for the population accumulated by the transition from neighboring ions, and τ_r is a rise-time constant defined as the time elapsed until emission intensity reaches $(1 - 1/e)$

of its maximum value. Taking it that $I \propto N$, the temporal dependence of emission intensity, $I(t)$, can be described by:

$$I(t) = \{A + B \cdot [1 - \exp(-t/\tau_d)]\} \cdot \exp(-t/\tau_d), \quad (23)$$

where τ_d is the decay constant, and A and B are intensity parameters.

Khalid and Kontis [132] have shown that it is possible to perform 2D-surface thermal imaging using the emission rise time of Eu^{3+} in Y_2O_3 ; however, the uncertainty of the measurement was relatively high. In addition, they reported (for the first time) that the time at which the emission reaches its maximum value ('time-to-max') can be used as an excellent read-out of temperature. Recently, Lojpur *et al* [133] have investigated the rise time of Eu^{3+} emission in SrY_2O_4 over the 298–473 K temperature range. In the 0.5 at% doped sample, the rise-time value linearly changed from 138 to 13 μs , as shown in figure 10(a), which corresponds to an absolute sensitivity of $0.66 \mu\text{s}\cdot\text{K}^{-1}$ over the complete temperature range and a quite high relative sensitivity of $5.53\%\text{K}^{-1}@473\text{K}$. In addition, the time-to-max temperature dependence was measured; the dependence was linear over the complete temperature range, and this read-out provided absolute and relative sensitivities of $1.29 \mu\text{s}\cdot\text{K}^{-1}$ and $0.64\%\text{K}^{-1}@473\text{K}$, respectively. Figure 10(b) shows the temporal behavior of Eu^{3+} emission in SrY_2O_4 at different temperatures. The emission rise time of $\text{BaY}_2\text{ZnO}_5:\text{Eu}^{3+}$ has been investigated by Li *et al* [134]; the rise-time value decreased from 207 μs at 330 K to 16 μs at 510 K, with corresponding absolute and relative sensitivities of $1.1 \mu\text{s}\cdot\text{K}^{-1}$ and $2.2\%\text{K}^{-1}@490\text{K}$.

It is important to note that the emission of Eu^{3+} was used in all reports, and that a relatively small number of reports have been published on rise-time thermometry despite the fact that this read-out scheme provides very good performance. Read-out of temperature from time-to-max values could be quite beneficial. First, unlike decay- or rise times which need data processing for their evaluation, time-to-max values can be read simply. Consequently, measurements of time are very accurate, so the time-to-max values can be determined with small measurement errors, which in combination with relatively large sensitivities, may provide luminescence temperature measurements with an excellent temperature resolution. However, the temperature resolution of the method has not been demonstrated yet in the literature. It should also be noted that the choice of dopant ion concentration is very important for this method. It has been shown [133, 134] that the rise-time value strongly reduces with an increase in dopant concentration and that thermometry with low-doped samples provides much better measurement ranges and sensitivity. On the other hand, emission intensity lessens with a decrease in dopant concentration, so the proper concentration should compromise between these two effects.

5. Multifunctional applicability of lanthanide luminescence

For the longest time in human history, the vast majority of materials have had only one function: to bear loads (to provide mechanical strength), and were known as structural materials. As time passed and human knowledge increased, new materials with novel functions were discovered, e.g. those capable of conducting electricity, emitting light, or showing thermal resistance, sometimes simultaneously. We are now witnessing a new phase in material research, where it is expected that materials and structures will perform several functions; it is reasonable to believe that in the near future most, if not all, materials and structures will be 'smart', 'tailored' multifunctional materials. These type of materials are designed to meet specific requirements through tailored physical properties which can change with the variation in certain external conditions; they can be defined as materials of specific properties favorable to meeting otherwise unattainable performance. Multifunctional design incorporates materials, structures and material systems that have the capacity to perform multiple functions through careful combinations of structural properties and at least one additional functional capability, as required by the system application.

Lanthanide-doped metal oxides and salts, as well as all luminescent materials, are ideal candidates for the development of multifunctional materials. This is because the luminescence of lanthanide ions is already used for a great number of diverse functions and host materials may have their own functional abilities. It is well known that lanthanide luminescence can be used for lasing, lighting, bio-labeling, imaging and counterfeiting, to name only a few important functions and applications. Luminescence changes its characteristics in the presence of chemical species or as a response to physical stimuli (temperature, pressure, electric and magnetic fields, radiation of high energy, etc). The host material may be ferromagnetic, ferroelectric or it can, for example, provide its pristine emission. With this in mind, it is reasonable to expect that with many well-known materials, multifunctionality (polyvalence) may be achieved by the addition of luminescent thermometric functionality. In addition, it is possible to create a completely new multifunctional material with thermometric function by designing a structure with adequate luminescent and other physical properties (at least one).

Among the very first multifunctional materials with added thermometric function were thermal and environmental barrier coatings. Through doping with lanthanide ions it was possible to measure the temperature of coatings at and below surfaces as well as under transient conditions [7]. More recently it has been shown that the ratio of green and red emissions of Er^{3+} (${}^2\text{H}_{11}$ and ${}^4\text{S}_{3/2} \rightarrow {}^4\text{I}_{15/2}$ transitions) ions doped in a ferroelectric BaTiO_3 host changes in an electric field when

Table 3. An overview of lanthanide-ion-doped metal oxides and salts used for decay-time read-out of temperature (abbreviations: *shape*: CT—coating, P—powder, NC—nanocrystal, C—crystal, F—fiber; *synthesis*: PCS—polymerized complex solution method, RFMS—radio frequency magnetron sputtering, CVD—chemical vapor deposition, EB-PVD—electron beam physical vapor deposition, BT—Bridgman technique).

Ion	Material	Shape	Synthesis	Range (K)	Sensitivity range (K)	Comments	Ref.
Eu ³⁺	Y ₂ O ₃	CT	PCS	293–1393	790–1390		[106]
Eu ³⁺	Y ₂ O ₃			720–1473	720–1473	Sensitive to oxygen	[107]
Eu ³⁺	Y ₂ O ₃	CT	RFMS	290–1370	700–1300	Thin and thick films	[108]
Eu ³⁺	Y ₂ O ₂ S	CT	Commercial	350–450	350–450	$4 \cdot 10^{-5}$ – $1 \cdot 10^{-6}$ s	[109]
Eu ³⁺	GdAlO ₃	P	Solid-state	293–793	620–793	$S_R = 2.28\%K^{-1}@793$ K	[59]
Eu ³⁺	LaOF	P	Combustion	293–700	423–623		[110]
Eu ³⁺	TiO ₂	NC	Sol-gel	307–533	307–500	$S_R = 2.43\%K^{-1}@400$ K	[92]
Eu ³⁺	Y ₃ Al ₅ O ₁₂	P	Solid-state	750–1470	1000–1470	$2 \cdot 10^{-3}$ – $2 \cdot 10^{-6}$ s	[111]
Eu ³⁺	YAlO ₃	P	Solid-state	750–1300	850–1300	$1 \cdot 10^{-3}$ – $2 \cdot 10^{-6}$ s	[111]
Eu ³⁺	YNbO ₄	P	Solid-state	303–800	620–773		[74]
Eu ³⁺	Gd ₂ O ₃	P	Combustion	10–800	600–800		[56]
Eu ³⁺	Gd ₂ O ₃	CT	CVD	300–1070	770–1070	$1 \cdot 10^{-3}$ – $3 \cdot 10^{-6}$ s	[112]
Eu ³⁺	Sc ₂ O ₃	CT	CVD	300–1270	970–1270	$1 \cdot 10^{-3}$ – $6 \cdot 10^{-6}$ s	[112]
Eu ³⁺	BaMgAl ₁₀ O ₁₇	P	Sol-gel	973–1473	973–1350	Eu ²⁺ /Eu ³⁺	[113]
Eu ³⁺	GdVO ₄	P	Solid-state	10–750	550–750		[37]
Eu ³⁺	TiO ₂	CT	Dip-coating	293–673	473–673	0.26–1.14% Eu ³⁺	[114]
Eu ³⁺	La ₂ O ₂ S			390–510	420–508	Insensitive to oxygen	[107]
Eu ³⁺	La ₂ O ₂ S			70–325	200–325	⁵ D ₂ for low <i>T</i>	[115]
				293–550	350–550	⁵ D ₁ for high <i>T</i>	
Eu ³⁺	YSZ ^a	CT	EB-PVD	300–1370	750–12370	$\tau : 1 \cdot 10^{-3}$ – $5 \cdot 10^{-8}$ s	[7]
Eu ³⁺	BSAS ^b			300–1700	700–1270	$\tau : 2 \cdot 10^{-6}$ – $1 \cdot 10^{-7}$ s	[7]
Eu ³⁺	Y ₂ SiO ₅	P	Co-precipitation	300–1470	870–1470	$\tau : 1 \cdot 10^{-3}$ – $3 \cdot 10^{-7}$ s	[116]
Eu ³⁺	CaMoO ₄	P	Solid-state	300–1000	600–1000	$\tau : 3 \cdot 10^{-4}$ – $4 \cdot 10^{-7}$ s	[117]
Eu ³⁺	LaPO ₄	P	Solid-state	300–1180	700–1180	$\tau : 3 \cdot 10^{-3}$ – $5 \cdot 10^{-7}$ s	[117]
Eu ³⁺	LaVO ₄	P	Solid-state	300–820	500–820	$\tau : 7 \cdot 10^{-4}$ – $7 \cdot 10^{-6}$ s	[117]
Eu ²⁺	BaMg ₂ Al ₁₀ O ₁₇	P	Commercial	290–1300	700–1300	$\tau : 1 \mu\text{s}$ –10 ns	[118]
Eu ²⁺	(Sr,Mg) ₂ SiO ₄ :Eu			290–720	500–700	$\tau : 5$ ns at 700 K	[118]
Dy ³⁺	GdVO ₄	P	Solid-state	10–600	480–600		[37]
Dy ³⁺	GdAlO ₅			300–1470	1170–1470	$\tau : 3 \cdot 10^{-4}$ – $4 \cdot 10^{-6}$ s	[7]
Dy ³⁺	Y ₃ Al ₅ O ₁₂	P	Commercial	290–1970	1370–1970	$\tau : 4 \cdot 10^{-4}$ – $2 \cdot 10^{-6}$ s	[119]
Dy ³⁺	Al ₂ O ₃	CT	Sol-gel	293–1473	1115–1473	Comb. with Cr ³⁺	[120]
Dy ³⁺	YSZ ^a	CT	EB-PVD	300–1350	670–1350	$\tau : 2 \cdot 10^{-4}$ – $3 \cdot 10^{-8}$ s	[7]
Dy ³⁺	Y ₂ SiO ₅	P	Co-precipitation	300–1700	1170–1700	$\tau : 7 \cdot 10^{-4}$ – $1 \cdot 10^{-6}$ s	[7]
Dy ³⁺	Y ₂ SiO ₅	P	Co-precipitation	300–1700	1170–1700	$\tau : 7 \cdot 10^{-4}$ – $1 \cdot 10^{-6}$ s	[7]
Dy ³⁺	BSAS ^b			300–1700	1270–1700	$\tau : 6 \cdot 10^{-4}$ – $1 \cdot 10^{-7}$ s	[7]
Sm ²⁺	BaClF	P	Solid-state	293–600	293–473	Silicon fiber	[121]
Sm ²⁺	BaFCl	C	BT	10–470	100–470	$\tau : 8 \cdot 10^{-4}$ – $5 \cdot 10^{-7}$ s	[122]
Sm ²⁺	CaFCl	C	BT	10–300	100–300	$\tau : 5 \cdot 10^{-5}$ – $2 \cdot 10^{-7}$ s	[122]
Sm ²⁺	SrFCl	C	BT	10–470	100–470	$\tau : 4 \cdot 10^{-4}$ – $3 \cdot 10^{-7}$ s	[122]
Sm ³⁺	YNbO ₄	P	Solid-state	303–773	620–750		[74]
Sm ³⁺	TiO ₂	NC	Sol-gel	297–383	300–370	$S_R = 10.15\%K^{-1}@340$ K	[94]
Sm ³⁺	Y ₂ O ₂ S	P	Commercial	400–1425	900–1425		[76]
Sm ³⁺	YSZ ^a	CT	EB-PVD	300–1300	300–1300	$\tau : 2 \cdot 10^{-3}$ – $5 \cdot 10^{-7}$ s	[7]
Pr ³⁺	CaTiO ₃	P	Solid-state	300–620	300–620	$\tau : 5 \cdot 10^{-5}$ – $3 \cdot 10^{-8}$ s	[117]
Tb ³⁺	CaMoO ₄	C	Flux	10–297	10–297		[123]
Tb ³⁺	CaWO ₄	C	Flux	10–297	10–297		[123]
Tb ³⁺	Y ₂ SiO ₅	P	Co-precipitation	300–1570	1220–1570	$\tau : 3 \cdot 10^{-3}$ – $3 \cdot 10^{-6}$ s	[7]
Tb ³⁺	BSAS ^b			300–1670	700–1670	⁵ D ₄ , ⁵ D ₃	[7]
Tb ³⁺	GdAlO ₃	P	Co-precipitation	300–1500	1070–1500	$\tau : 2 \cdot 10^{-3}$ – $1 \cdot 10^{-7}$ s	[124]
Tm ³⁺	Y ₃ Al ₅ O ₁₂	P	Commercial	290–1770	1270–1770	Up to 1970 K doped with Dy ³⁺ /Tm ³⁺	[119]
Tm ³⁺	Al ₂ O ₃	CT	Sol-gel	293–1473	1157–1473	Could be comb. with Cr ³⁺	[120]

(Continued)

Table 3. (Continued)

Ion	Material	Shape	Synthesis	Range (K)	Sensitivity range (K)	Comments	Ref.
Nd ³⁺	YVO ₄			298–1123	970–1123	$S = 0.13 \mu\text{s K}^{-1}$ (>970 K)	[125]
Nd ³⁺	KGd(WO ₄) ₂			298–1023	870–1023	$S = 0.5 \mu\text{s K}^{-1}$ (>870 K)	[125]
Nd ³⁺	Y ₃ Al ₅ O ₁₂			298–1273	920–1273	$S = 0.27 \mu\text{s K}^{-1}$ (>920 K)	[125]
Nd ³⁺	Y ₃ Al ₅ O ₁₂	C		300–1100	900–1100		[126]
Nd ³⁺	Y ₃ Al ₅ O ₁₂			300–488	300–488		[127]
Nd ³⁺	Nd/Al/SiO ₂	CT		273–1000	273–1000	Linear T -dependence	[125]
Nd ³⁺	YP ₅ O ₁₄	P	Hydrothermal	77–700	400–700		[128]

^aYSZ—yttria-stabilized zirconia (Y_{0.076}Zr_{0.924}O_{1.962}).

^bBSAS—barium-strontium aluminosilicate ((Ba_{0.75}Sr_{0.25})Al₂Si₂O₈).

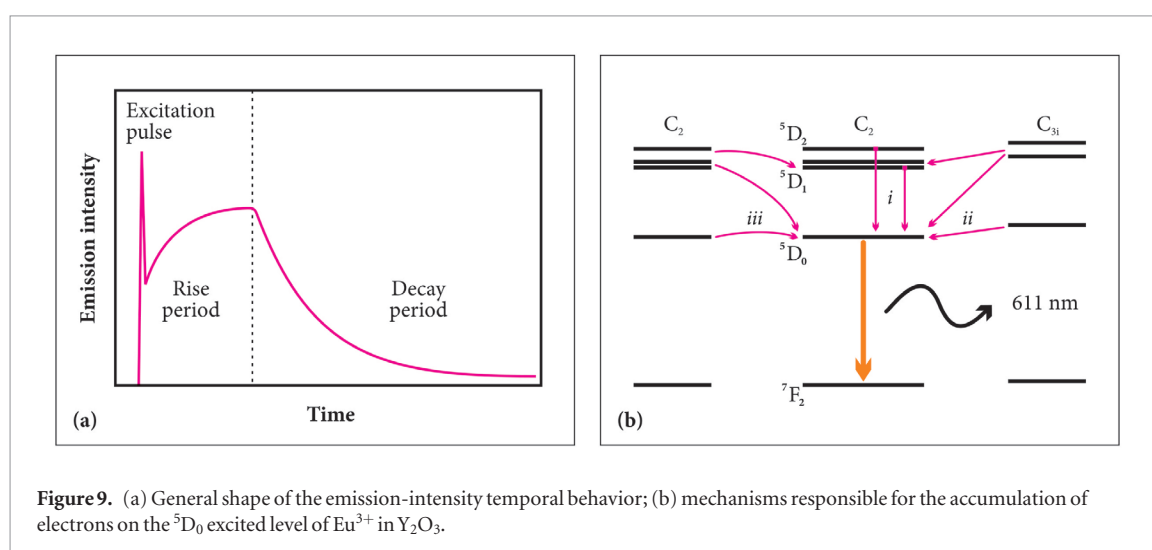


Figure 9. (a) General shape of the emission-intensity temporal behavior; (b) mechanisms responsible for the accumulation of electrons on the ⁵D₀ excited level of Eu³⁺ in Y₂O₃.

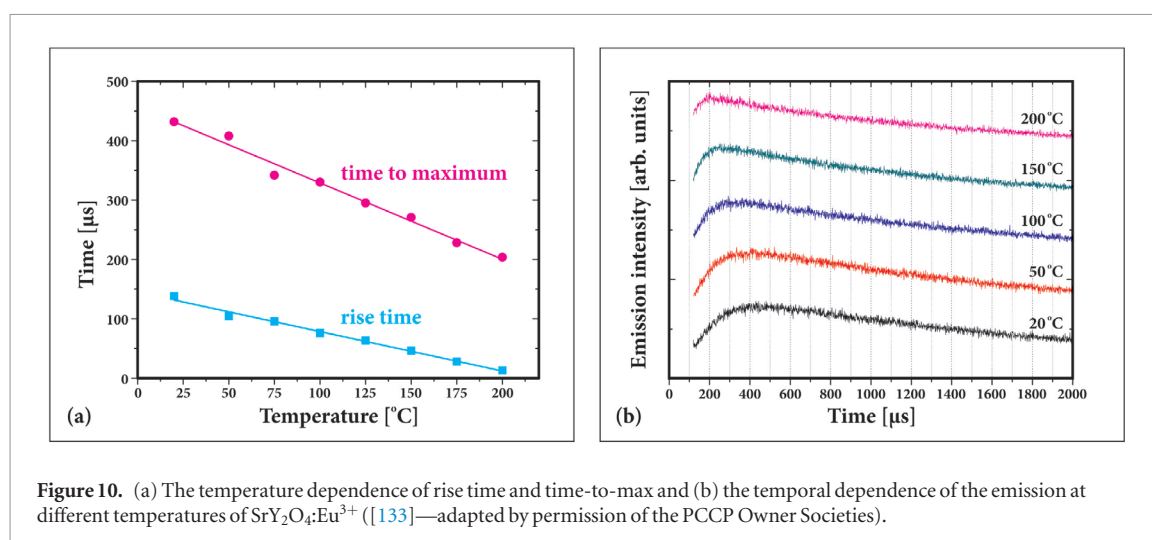
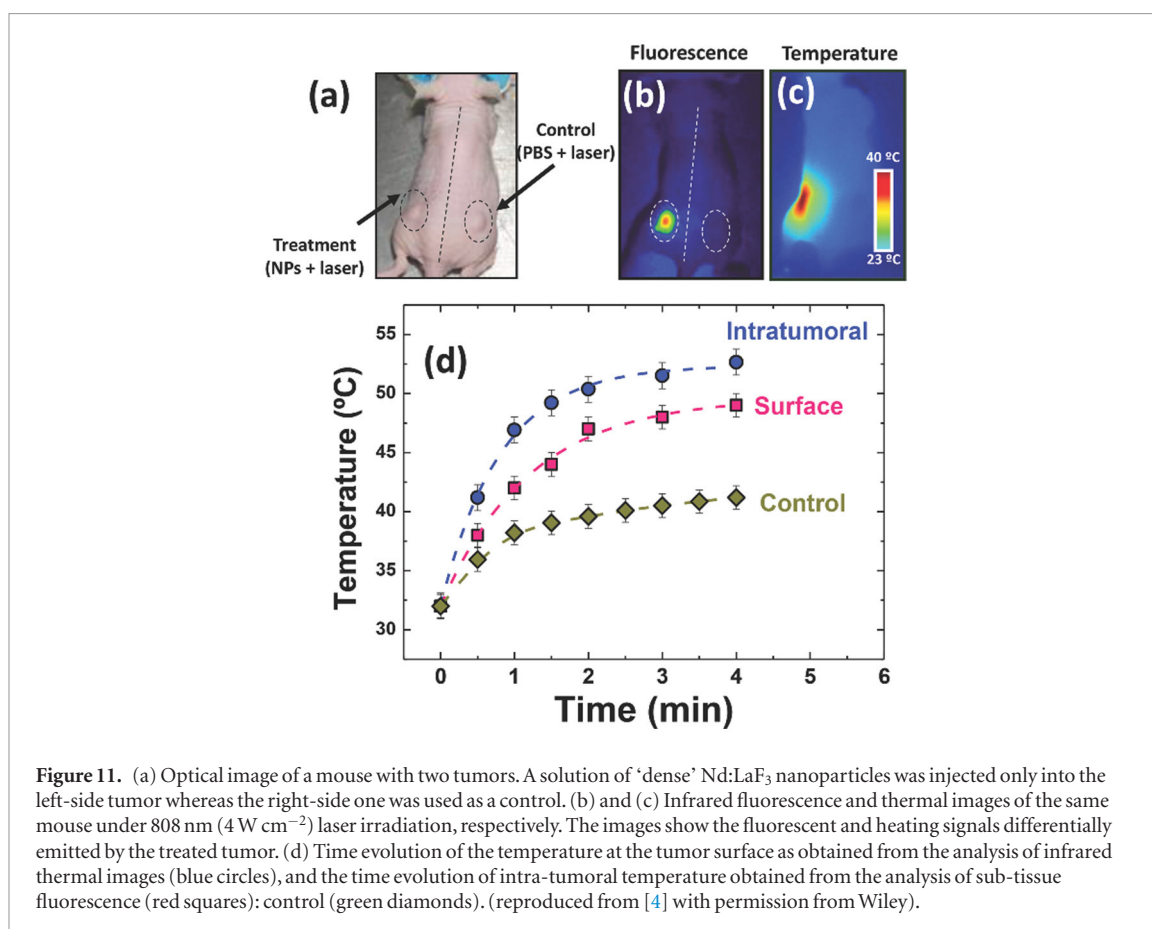


Figure 10. (a) The temperature dependence of rise time and time-to-max and (b) the temporal dependence of the emission at different temperatures of SrY₂O₄:Eu³⁺ ([133])—adapted by permission of the PCCP Owner Societies.

the field intensity changes [135]. The ratio of these emissions is exactly that which is used in LIR thermometry for both downshifting and upconversion emissions. When Gd³⁺ ions are constituents of the host matrix the material exhibits paramagnetic properties and it is able to sense magnetic fields. It has been shown [136, 137] that GdVO₄ nanoparticles can act as T₁-positive contrast agents for magnetic resonance imaging (MRI) because Gd³⁺ ions possess unpaired electrons that efficiently alter the relaxation time of the surrounding water protons, and that they also provide luminescence

imaging and controlled drug release functionalities. Gavrilović *et al* [138] have added thermometric functionality to ultra-small GdVO₄ nanoparticles after doping with Er³⁺ ions. The LIR method, which uses the emissions from ²H_{11/2} and ⁴S_{3/2} → ⁴I_{15/2} transitions provided thermometry over the 307–473 K range, with a relative sensitivity of 1.11%K⁻¹ at 307 K and a temperature resolution of better than 1 K. The emission of Er³⁺ in Gd₂O₃ nanoparticles exhibits a strong decrease in intensity when nanoparticles are placed in a magnetic field [139]. However, the ratio of ²H_{11/2} and



$^4S_{3/2} \rightarrow ^4I_{15/2}$ emissions remains the same at a constant temperature, meaning that these nanoparticles are able to selectively sense both the intensity of the magnetic field (from the emission intensity) and the temperature (from emission intensity ratio). Nikolić *et al* [63] have showed that Eu³⁺-doped (Y_{0.75}Gd_{0.25})₂O₃ scintillating powder is capable of measuring temperature over the 293–773 K range from the ratio of ⁵D₁ and ⁵D₀ emissions that were excited by high energy radiation. Recently, Carrasco *et al* [4] have demonstrated Nd³⁺ ion-doped LaF₃ nanoparticles capable of *in vivo* photothermal heating, fluorescent tumor localization and intratumoral temperature sensing, figure 11.

6. Concluding remarks

The luminescence thermometry field of research has continuously grown over the past few years. This growth is manifested by an increased number of publications in international scientific journals and by many cutting-edge applications. Today, luminescence thermometry is the most developed method among optical thermometries, leaving aside traditional pyrometry. Lanthanide-doped metal oxides and salts were among the first investigated probes, and even today are frequently the materials of choice. Thermometry may exploit both the downshifting emission, in the visible spectrum, but also in NIR, and upconversion emission of these materials, the latter of which has received particular attention in recent years.

However, downshifting emissions of lanthanide ions are considerably more efficient and deliver stronger signals than upconversion emissions. Therefore, better signal-to-noise ratios and smaller uncertainties may be expected in downshifting- than in upconversion-based thermometry. Sensitivity of upconversion-based thermometry is affected by measurement conditions. For example, it depends on the intensity of excitation, as recently demonstrated by Marciniak *et al* [140]; the effect may be discussed in terms of competition between thermalization and nonradiative depopulation processes. In addition, downshifting emission decays are quite frequently of single exponential nature, contrary to upconversion, which makes the interpretation of data easier. On the other hand, upconversion emission is excited by NIR radiation, thus enabling applications in biology and medicine.

Temperature was most frequently read from lifetimes of downshifting luminescence in the early stage of development of luminescence thermometry; developments at that time were mostly aimed at applications at high-temperatures. More recently, the research focus has shifted to time-integrated methods, especially to the LIR method, and to the physiologically relevant temperature range. Both approaches present some advantages over each other. The LIR technique is found to be faster, simpler and requires less sophisticated instrumentation than the lifetime method and, therefore, it has received more attention lately. Generally, LIR methods present larger relative sensitivities than lifetime ones. On

the other hand, to be self-referencing, lifetime methods require the monitoring of just one emission while time-integrated methods require the monitoring of two distinctively separated emissions. Measurements of temporal-emission changes are generally more accurate than emission-intensity measurements. Better values of uncertainties compensate for lower sensitivities, so time-resolved methods may provide better temperature resolution than the LIR ones [92, 96]. Lifetime methods suffer from small operating ranges and the low-temperature bound can be at a relatively high temperature in a lot of cases. This obstacle may be overcome by the reading of temperature from the rise times. The high-temperature bound, on the other hand, is generally at higher temperatures in lifetime methods than in LIR. But, the performance of thermometry that uses materials with a single emission center, in both time-resolved and time-integrated approaches, is mostly governed by the intrinsic luminescence properties of the dopant lanthanide ion with a fair contribution from the host material characteristics. The relative sensitivity of LIR that uses emissions from the thermally coupled excited levels of lanthanide ions is directly proportional to the energy gap between these levels. The largest energy gap is the one in the Eu^{3+} ion of about 1750 cm^{-1} , meaning that relative sensitivity varies with temperature as $\sim 251\ 800/T$ ($\%K^{-1}$) and that the maximum achievable theoretical relative sensitivity of the technique is around $S_{R\text{max}} \sim 2.8\%K^{-1}$ at 300 K for different hosts. Bearing this in mind, and considering the large number of publications that have reported on LIR thermometry with different ion/host combinations, it is not reasonable to expect that further research focused simply on the scrutiny of performance of different combinations of a single lanthanide luminescence centers and hosts will bring about any progress in the field. However, this LIR method can be further developed by improving its temperature resolution, which is rather low and rarely better than 1 K. This can be accomplished by enhancing measurement signals which would yield larger absolute sensitivities (if the signal-to-noise ratio is maintained) and/or by improving signal-to-noise and measurement procedures to lower the measurement uncertainties.

Further improvement in LIR relative sensitivities may be expected with the use of multiple emission centers, as discussed in section 3.2. These centers may be all lanthanide ions or a combination of lanthanide ions and other types of emission centers. Such probes may also provide multiple read-outs of temperature which, when combined, give wider operating ranges with good relative sensitivity and resolution. We should also note that the investigations into thermometry that use NIR emissions have just begun, and that they have potentially valuable applications especially in biomedicine.

Selection of materials for the luminescence thermometry probes ought to be done for the specific application. In this sense, measurement environment, temperature range of interest, adequate temperature resolution, the price of material and its availability,

as well some other material properties determine the selection. Different types of materials provide different advantages, but also disadvantages. Regarding thermometry via downshifting emission, for example, lanthanide temperature probes containing organic ligands may be advantageous over lanthanide-doped metals and salts since their absorptions are much increased owing to organic ligands that act as antennas, and because excitation wavelengths are shifted into the visible spectral region. The later property can significantly reduce autofluorescence when investigating the temperature properties of tissues. On the other hand, these probes have substantially lower temperature and chemical stability than inorganic ones, limiting their use at high temperatures and in harsh environments. In addition, metal oxides and salts doped with lanthanide ions are excellent platforms for the development of multifunctional materials, considering the variety of important uses of lanthanide luminescence and the different functionalities of host materials in which lanthanide ions can be introduced. As mentioned at the beginning of this text, knowing that temperature is essential in almost all aspects of human activities, and by providing thermometric functionalities to existing or new materials systems, this could lead to exciting progress in many disciplines. Some of them are briefly mentioned in the text and include dual- or multi-sensing devices, multimodal imaging with temperature monitoring and temperature-supervised photothermal therapies.

Acknowledgments

The author is grateful to Dr Vesna Đorđević, Dr Sanja Čulubrk, Dr Dragana Jovanović, and Dr Željka Antić for their help in systematizing the presented data, and to Dr Radenka Krsmanović Whiffen and Dr Vesna Đorđević for critically reading the manuscript. This work is supported by the Ministry of Education, Science and Technological Development of the Republic of Serbia (Grant number 171022). The funders had no role in study design, data collection and analysis, decision to publish, or preparation of the manuscript.

References

- [1] Machin G and Tsai B K 2010 Temperature fundamentals *Radiometric Temperature Measurements I. Fundamentals* ed Z M Zhang *et al* (New York: Academic) pp 29–71
- [2] Childs P R N 2001 Temperature *Practical Temperature Measurement* ed P R N Childs (Oxford: Butterworth-Heinemann) pp 1–15
- [3] Childs P R N, Greenwood J R and Long C A 2000 Review of temperature measurement *Rev. Sci. Instrum.* **71** 2959–78
- [4] Carrasco E, del Rosal B, Sanz-Rodríguez F, de la Fuente Á J, Gonzalez P H, Rocha U, Kumar K U, Jacinto C, Solé J G and Jaque D 2015 Intratumoral thermal reading during photothermal therapy by multifunctional fluorescent nanoparticles *Adv. Funct. Mater.* **25** 615–26
- [5] Khalid A H and Kontis K 2008 Thermographic phosphors for high temperature measurements: principles, current state of the art and recent applications *Sensors* **8** 5673–744

- [6] Allison S W and Gillies G T 1997 Remote thermometry with thermographic phosphors: instrumentation and applications *Rev. Sci. Instrum.* **68** 2615–50
- [7] Chambers M D and Clarke D R 2009 Doped oxides for high-temperature luminescence and lifetime thermometry *Annu. Rev. Mater. Res.* **39** 325–59
- [8] McLaurin E J, Bradshaw L R and Gamelin D R 2013 Dual-emitting nanoscale temperature sensors *Chem. Mater.* **25** 1283–92
- [9] Jaque D and Vetrone F 2012 Luminescence nanothermometry *Nanoscale* **4** 4301–26
- [10] Brites C D S, Lima P P, Silva N J O, Millán A, Amaral V S, Palacio F and Carlos L D 2012 Thermometry at the nanoscale *Nanoscale* **4** 4799–829
- [11] Wang X, Wolfbeis O S and Meier R J 2013 Luminescent probes and sensors for temperature *Chem. Soc. Rev.* **42** 7834–69
- [12] Fischer L H, Harms G S and Wolfbeis O S 2011 Upconverting nanoparticles for nanoscale thermometry *Angew. Chem., Int. Ed. Engl.* **50** 4546–51
- [13] Heyes A L 2009 On the design of phosphors for high-temperature thermometry *J. Lumin.* **129** 2004–9
- [14] Aldén M, Omrane A, Richter M and Särner G 2011 Thermographic phosphors for thermometry: a survey of combustion applications *Prog. Energy Combust. Sci.* **37** 422–61
- [15] Pandey A and Rai V K 2011 Rare earth doped materials for temperature sensors *Spectroscopic Techniques for Security Forensic and Environmental Applications* ed Y Dwivedi *et al* (New York: Nova Science Publishers) pp 279–92
- [16] Grattan K T V and Zhang Z Y 1994 Fiber optic fluorescence thermometry *Topics in Fluorescence Spectroscopy: Probe Design and Chemical Sensing* ed J R Lakowicz (Boston, MA: Springer) pp 335–76
- [17] Pérez-Prieto M and González-Béjar J 2015 Upconversion luminescent nanoparticles in physical sensing and in monitoring physical processes in biological samples *Methods Appl. Fluoresc.* **3** 42002
- [18] McSherry M, Fitzpatrick C and Lewis E 2005 Review of luminescent based fibre optic temperature sensors *Sens. Rev.* **25** 56–62
- [19] Brübach J, Pflitsch C, Dreizler A and Atakan B 2013 On surface temperature measurements with thermographic phosphors: a review *Prog. Energy Combust. Sci.* **39** 37–60
- [20] Reddy B R, Kamma I and Kommidu P 2013 Optical sensing techniques for temperature measurement *Appl. Opt.* **52** B33–9
- [21] Wade S A, Collins S F and Baxter G W 2003 Fluorescence intensity ratio technique for optical fiber point temperature sensing *J. Appl. Phys.* **94** 4743–56
- [22] Brites C D S, Lima P P, Silva N J O, Millán A, Amaral V S, Palacio F and Carlos L D 2011 Lanthanide-based luminescent molecular thermometers *New J. Chem.* **35** 1177–83
- [23] Wang X, Liu Q, Bu Y, Liu C-S, Liu T and Yan X 2015 Optical temperature sensing of rare-earth ion doped phosphors *RSC Adv.* **5** 86219–36
- [24] de Menezes L S and de Araújo C B 2015 Optically detected thermal effects in rare-earth doped materials for host characterization, thermometric devices, nanothermometry and biothermometry *J. Braz. Chem. Soc.* **26** 2405–17
- [25] Zhou H, Sharma M, Berezin O, Zuckerman D and Berezin M Y 2016 Nanothermometry: from microscopy to thermal treatments *ChemPhysChem* **17** 27–36
- [26] Grattan K T V and Zhang Z 1995 *Fiber Optic Fluorescence Thermometry* (London: Chapman and Hall)
- [27] Carlos L D and Palacio F 2015 *Thermometry at the Nanoscale* ed L Carlos and F Palacio (Cambridge, MA: Royal Society of Chemistry)
- [28] Cates M R, Allison S W, Jaiswal S L and Beshears D L 2003 YAG:Dy and YAG:Tm fluorescence to 1700 C *ISA Int. Instrum. Symp. 49th (Orlando)*
- [29] Yen W M, Shionoya S and Yamamoto H 2007 *Phosphor Handbook* (Boca Raton, FL: CRC Press)
- [30] Lakowicz J R 2006 Introduction to Fluorescence *Principles of Fluorescence Spectroscopy* (Boston, MA: Springer) pp 1–26
- [31] Strickler S J and Berg R A 1962 Relationship between absorption intensity and fluorescence lifetime of molecules *J. Chem. Phys.* **37** 814–22
- [32] Blasse G 1976 The influence of charge-transfer and rydberg states on the luminescence properties of lanthanides and actinides *Spectra and Chemical Interactions* ed P S Braterman *et al* (Berlin: Springer) pp 43–79
- [33] Klick C C and Schulman J H 1957 Luminescence in solids *Solid State Phys.* **5** 97–172
- [34] Riseberg L A and Moos H W 1968 Multiphonon orbit-lattice relaxation of excited states of rare-earth ions in crystals *Phys. Rev.* **174** 429–38
- [35] Riseberg L A and Weber M J 1977 Relaxation phenomena in rare-earth luminescence *Prog. Opt.* **14** 89–159
- [36] Moos H W 1970 Spectroscopic relaxation processes of rare earth ions in crystals *J. Lumin.* **1–2** 106–21
- [37] Nikolić M G, Jovanović D J and Dramićanin M D 2013 Temperature dependence of emission and lifetime in Eu^{3+} - and Dy^{3+} -doped GdVO_4 *Appl. Opt.* **52** 1716–24
- [38] Voron'ko Y K, Sobol' A A, Shukshin V E, Zagumennyi A I, Zavartsev Y D and Kutovoi S A 2009 Raman spectroscopic study of structural disordering in YVO_4 , GdVO_4 , and CaWO_4 crystals *Phys. Solid State* **51** 1886–93
- [39] Blasse G 1966 On the Eu^{3+} Fluorescence of mixed metal oxides. IV. The photoluminescence efficiency of Eu^{3+} -activated oxides *J. Chem. Phys.* **45** 2356–60
- [40] Fonger W H and Struck C W 1970 Eu^{+3}D Resonance quenching to the charge-transfer states in Y_2O_3 , La_2O_3 , and LaOCl *J. Chem. Phys.* **52** 6364–72
- [41] Struck C W and Fonger W H 1976 Quantum-mechanical treatment of $\text{Eu}^{3+} 4f \rightarrow 4f$ and $4f \rightarrow$ charge-transfer-state transitions in Y_2O_3 and La_2O_3 *J. Chem. Phys.* **64** 1784–90
- [42] Englman R and Jortner J 1970 The energy gap law for radiationless transitions in large molecules *Mol. Phys.* **18** 145–64
- [43] Kusama H, Sovers O J and Yoshioka T 1976 Line shift method for phosphor temperature measurements *Japan. J. Appl. Phys.* **15** 2349–58
- [44] Rocha U *et al* 2013 Subtissue thermal sensing based on neodymium-doped LaF_3 nanoparticles *ACS Nano* **7** 1188–99
- [45] Peng H, Song H, Chen B, Wang J, Lu S, Kong X and Zhang J 2003 Temperature dependence of luminescent spectra and dynamics in nanocrystalline $\text{Y}_2\text{O}_3:\text{Eu}^{3+}$ *J. Chem. Phys.* **118** 3277–82
- [46] Wang X, Zheng J, Xuan Y and Yan X 2013 Optical temperature sensing of $\text{NaYbF}_4:\text{Tm}^{3+}@\text{SiO}_2$ core-shell micro-particles induced by infrared excitation *Opt. Express* **21** 21596–606
- [47] Quintanilla M, Benayas A, Naccache R, Vetrone F, Quintanilla M, Benayas A, Naccache R and Vetrone F 2015 Luminescent nanothermometry with lanthanide-doped nanoparticles *Thermometry at the Nanoscale: Techniques and Selected Applications* ed L D Carlos and F Palacio (London: Royal Society of Chemistry) pp 124–66
- [48] Čulubrk S, Lojpur V, Ahrenkiel S P, Nedeljković J M and Dramićanin M D 2016 Non-contact thermometry with Dy^{3+} doped $\text{Gd}_2\text{Ti}_2\text{O}_7$ nano-powders *J. Lumin.* **170** 395–400
- [49] Lojpur M, Nikolić G, Dramićanin M D 2014 Luminescence thermometry below room temperature via up-conversion emission of $\text{Y}_2\text{O}_3:\text{Yb}^{3+}, \text{Er}^{3+}$ nanophosphors *J. Appl. Phys.* **115** 203106
- [50] Liu L, Creten S, Firdaus Y, Agustín Flores Cuautle J J, Kouyaté M, Van der Auweraer M and Glorieux C 2014 Fluorescence spectra shape based dynamic thermometry *Appl. Phys. Lett.* **104** 031902
- [51] Working Group 1 of the Joint Committee for Guides in Metrology (JCGM/WG 1) 2008 *Evaluation of Measurement Data—Guide to the Expression of Uncertainty in Measurement (JCGM 100:2008)* (Paris: Bureau International des Poids et Mesures) (www.bipm.org/en/publications/guides/gum.html)
- [52] Joint Committee for Guides in Metrology (JCGM) 2008 *International Vocabulary of Metrology—Basic and General Concepts and Associated Terms (VIM) (JCGM 200:2008)* 3rd edn (Paris: Bureau International des Poids et Mesures) (www.bipm.org/en/publications/guides/vim.html)

- [53] Brites C, Pereira P, João N, Millán A, Amaral V, Palacio F and Carlos L A D 2013 Organic–inorganic $\text{Eu}^{3+}/\text{Tb}^{3+}$ codoped hybrid films for temperature mapping in integrated circuits *Front. Chem.* **1** 9
- [54] Kim K, Jeong W, Lee W and Reddy P 2012 Ultra-high vacuum scanning thermal microscopy for nanometer resolution quantitative thermometry *ACS Nano* **6** 4248–57
- [55] Liang Z, Qin F, Zheng Y, Zhang Z and Cao W 2016 Noncontact thermometry based on downshifting luminescence from Eu^{3+} doped LiNbO_3 single crystal *Sensors Actuators A* **238** 215–9
- [56] Nikolić M G, Al-Juboori A Z, Đorđević V and Dramićanin M D 2013 Temperature luminescence properties of Eu^{3+} -doped Gd_2O_3 phosphors *Phys. Scr.* **T157** 014056
- [57] Tian Y, Tian B, Cui C, Huang P, Wang L and Chen B 2014 Excellent optical thermometry based on single-color fluorescence in spherical NaEuF_4 phosphor *Opt. Lett.* **39** 4164–7
- [58] Lojpur V, Antić Ž, Krsmanović R, Medić M, Nikolić M G and Dramićanin M D 2012 Thermographic properties of Eu^{3+} - and Sm^{3+} -doped Lu_2O_3 nanophosphor *J. Serb. Chem. Soc.* **77** 1735–46
- [59] Lojpur V, Čulubrk S, Medić M and Dramićanin M D 2016 Luminescence thermometry with Eu^{3+} doped GdAlO_3 *J. Lumin.* **170** 467–71
- [60] Meert K W, Morozov V A, Abakumov A M, Hadermann J, Poelman D and Smet P F 2014 Energy transfer in Eu^{3+} doped scheelites: use as thermographic phosphor *Opt. Express* **22** A961–72
- [61] Lojpur V, Čulubrk S and Dramićanin M D 2016 Ratiometric luminescence thermometry with different combinations of emissions from Eu^{3+} doped $\text{Gd}_2\text{Ti}_2\text{O}_7$ nanoparticles *J. Lumin.* **169** 534–8
- [62] Đačanin L R, Dramićanin M D, Lukić-Petrović S R, Petrović D M and Nikolić M G 2013 Eu^{3+} doped YNbO_4 phosphor properties for fluorescence thermometry *Radiat. Meas.* **56** 143–6
- [63] Nikolić M G, Lojpur V, Antić Ž and Dramićanin M D 2013 Thermographic properties of a Eu^{3+} -doped $(\text{Y}_{0.75}\text{Gd}_{0.25})_2\text{O}_3$ nanophosphor under UV and x-ray excitation *Phys. Scr.* **87** 055703
- [64] Rai K V and Rai A 2007 Temperature sensing behavior of Eu^{3+} doped tellurite and calibo glasses *Appl. Phys. B* **86** 333–5
- [65] Cao Z, Zhou S, Jiang G, Chen Y, Duan C and Yin M 2014 Temperature dependent luminescence of Dy^{3+} doped BaYF_3 nanoparticles for optical thermometry *Curr. Appl. Phys.* **14** 1067–71
- [66] Rakov N, Bispo L R A and Maciel G S 2012 Temperature sensing performance of dysprosium doped aluminum oxide powders *Opt. Commun.* **285** 1882–4
- [67] Chong J-Y, Zhang Y, Wagner B K and Kang Z 2013 Co-precipitation synthesis of YAG:Dy nanophosphor and its thermometric properties *J. Alloys Compd.* **581** 484–7
- [68] Heyes A L, Seefeldt S and Feist J P 2006 Two-colour phosphor thermometry for surface temperature measurement *Opt. Laser Technol.* **38** 257–65
- [69] Hasegawa R, Sakata I, Yanagihara H, Johansson B, Omrane A and Aldén M 2007 Two-dimensional gas-phase temperature measurements using phosphor thermometry *Appl. Phys. B* **88** 291–6
- [70] Kwong W Y, Steinberg A and Chin Y H 2014 Effect of $\text{B}^{3+}-\text{N}^{3-}$ on YAG:Dy thermographic phosphor luminescence *Opt. Lett.* **39** 6166–9
- [71] Boruc Z, Kaczkan M, Fetlinski B, Turczynski S and Malinowski M 2012 Blue emissions in Dy^{3+} doped $\text{Y}_4\text{Al}_2\text{O}_9$ crystals for temperature sensing *Opt. Lett.* **37** 5214–6
- [72] Antić Ž, Dramićanin M D, Prashanthi K, Jovanović D, Kuzman S, Thundat T 2016 Pulsed laser deposited dysprosium-doped gadolinium–vanadate thin films for noncontact, self-referencing luminescence thermometry *Adv. Mater.* **28** 7745–52
- [73] Bu Y Y, Cheng S J, Wang X F and Yan X H 2015 Optical thermometry based on luminescence behavior of Dy^{3+} -doped transparent LaF_3 glass ceramics *Appl. Phys. A* **121** 1171–8
- [74] Đačanin L R, Lukić-Petrović S R, Petrović D M, Nikolić M G and Dramićanin M D 2014 Temperature quenching of luminescence emission in Eu^{3+} - and Sm^{3+} -doped YNbO_4 powders *J. Lumin.* **151** 82–7
- [75] Nikolić M G, Jovanović D J, Đorđević V, Antić Ž, Krsmanović R M and Dramićanin M D 2012 Thermographic properties of Sm^{3+} -doped GdVO_4 phosphor *Phys. Scr.* **T149** 014063
- [76] Feist J P and Heyes A L 2000 The characterization of $\text{Y}_2\text{O}_3:\text{Sm}$ powder as a thermographic phosphor for high temperature applications *Meas. Sci. Technol.* **11** 942–7
- [77] Balabhadra S, Debasu M L, Brites C D S, Nunes L A O, Malta O L, Rocha J, Bettinelli M and Carlos L D 2015 Boosting the sensitivity of Nd^{3+} -based luminescent nanothermometers *Nanoscale* **7** 17261–7
- [78] Tian X, Wei X, Chen Y, Duan C and Yin M 2014 Temperature sensor based on ladder-level assisted thermal coupling and thermal-enhanced luminescence in $\text{NaYF}_4:\text{Nd}^{3+}$ *Opt. Express* **22** 30333–45
- [79] Jiang G, Wei X, Zhou S, Chen Y, Duan C and Yin M 2014 Neodymium doped lanthanum oxysulfide as optical temperature sensors *J. Lumin.* **152** 156–9
- [80] Jaque D and Jacinto C 2016 Luminescent nanoprobes for thermal bio-sensing: towards controlled photo-thermal therapies *J. Lumin.* **169** 394–9
- [81] Wawrzynczyk D, Bednarkiewicz A, Nyk M, Strek W and Samoc M 2012 Neodymium(III) doped fluoride nanoparticles as non-contact optical temperature sensors *Nanoscale* **4** 6959–61
- [82] Marciniak L, Prorok K, Bednarkiewicz A, Kowalczyk A, Hreniak D and Strek W 2016 Water dispersible $\text{LiNdP}_4\text{O}_{12}$ nanocrystals: new multifunctional NIR–NIR luminescent materials for bio-applications *J. Lumin.* **176** 144–8
- [83] Benayas A, del Rosal B, Pérez-Delgado A, Santacruz-Gómez K, Jaque D, Hirata G A and Vetrone F 2015 $\text{Nd}:\text{YAG}$ near-infrared luminescent nanothermometers *Adv. Opt. Mater.* **3** 687–94
- [84] Kolesnikov I E, Golyeva E V, Kurochkin M A, Lähderanta E and Mikhailov M D 2016 Nd^{3+} -doped YVO_4 nanoparticles for luminescence nanothermometry in the first and second biological windows *Sensors Actuators B* **235** 287–93
- [85] Pérez-Rodríguez C, Martín L L, León-Luis S F, Martín I R, Kumar K K and Jayasankar C K 2014 Relevance of radiative transfer processes on Nd^{3+} doped phosphate glasses for temperature sensing by means of the fluorescence intensity ratio technique *Sensors Actuators B* **195** 324–31
- [86] Wade S A, Muscat J C, Collins S F and Baxter G W 1999 Nd^{3+} -doped optical fiber temperature sensor using the fluorescence intensity ratio technique *Rev. Sci. Instrum.* **70** 4279–82
- [87] Tang W, Wang S, Li Z, Sun Y, Zheng L, Zhang R, Yang B, Cao W and Yu M 2016 Ultrahigh-sensitive optical temperature sensing based on ferroelectric Pr^{3+} -doped $(\text{K}_{0.5}\text{Na}_{0.5})\text{NbO}_3$ *Appl. Phys. Lett.* **108** 061902
- [88] Zhou S, Jiang G, Wei X, Duan C, Chen Y and Yin M 2014 Pr^{3+} -Doped $\beta\text{-NaYF}_4$ for temperature sensing with fluorescence intensity ratio technique *J. Nanosci. Nanotechnol.* **14** 3739–42
- [89] Rai V K and Rai S B 2007 A comparative study of FIR and FL based temperature sensing schemes: an example of Pr^{3+} *Appl. Phys. B* **87** 323–5
- [90] Rai V K, Rai D K and Rai S B 2006 Pr^{3+} doped lithium tellurite glass as a temperature sensor *Sensors Actuators A* **128** 14–7
- [91] Shen Y, Wang X, He H, Lin Y and Nan C-W 2012 Temperature sensing with fluorescence intensity ratio technique in epoxy-based nanocomposite filled with Er^{3+} -doped 7YSZ *Compos. Sci. Technol.* **72** 1008–11
- [92] Nikolić M G, Antić Ž, Čulubrk S, Nedeljković J M and Dramićanin M D 2014 Temperature sensing with Eu^{3+} doped TiO_2 nanoparticles *Sensors Actuators B* **201** 46–50
- [93] Lojpur V, Nikolić M G, Jovanović D, Medić M, Antić Ž and Dramićanin M D 2013 Luminescence thermometry with $\text{Zn}_2\text{SiO}_4:\text{Mn}^{2+}$ powder *Appl. Phys. Lett.* **103** 141912
- [94] Dramićanin M D, Antić Ž, Čulubrk S, Ahrenkiel S P and Nedeljković J M 2014 Self-referenced luminescence thermometry with Sm^{3+} doped TiO_2 nanoparticles *Nanotechnology* **25** 485501

- [95] Abazović N D, Comor M I, Dramićanin M D, Jovanović D J, Ahrenkiel S P and Nedeljković J M 2006 Photoluminescence of anatase and rutile TiO₂ particles *J. Phys. Chem. B* **110** 25366–70
- [96] Das S, Som S, Yang C-Y, Chavhan S and Lu C-H 2016 Structural evaluations and temperature dependent photoluminescence characterizations of Eu³⁺-activated SrZrO₃ hollow spheres for luminescence thermometry applications *Sci. Rep.* **6** 25787
- [97] Aizawa H, Katsumata T, Komuro S, Morikawa T, Ishizawa H and Toba E 2006 Fluorescence thermometer based on the photoluminescence intensity ratio in Tb doped phosphor materials *Sensors Actuators A* **126** 78–82
- [98] Tripathi G, Rai V K and Rai S B 2006 Optical properties of Sm³⁺:CaO–Li₂O–B₂O₃–BaO glass and codoped Sm³⁺:Eu³⁺ *Appl. Phys. B* **84** 459–64
- [99] Pandey A and Rai V K 2013 Optical thermometry using FIR of two close lying levels of different ions in Y₂O₃: Ho³⁺–Tm³⁺–Yb³⁺ phosphor *Appl. Phys. B* **113** 221–5
- [100] Ding M, Zhang H, Chen D, Junhua Xi Q H and Ji Z 2016 Color-tunable luminescence, energy transfer and temperature sensing behavior of hexagonal NaYF₄:Ce³⁺/Tb³⁺/Eu³⁺ microcrystals *J. Alloys Compd.* **672** 117–24
- [101] Marciniak L and Bednarkiewicz A 2016 The influence of dopant concentration on temperature dependent emission spectra in LiLa_{1-x-y}Eu_xTb_yP₄O₁₂ nanocrystals: toward rational designing of highly-sensitive luminescent nanothermometers *Phys. Chem. Chem. Phys.* **18** 15584–92
- [102] Marciniak L, Prorok K, Francés-Soriano L, Pérez-Prieto J and Bednarkiewicz A 2016 A broadening temperature sensitivity range with a core–shell YbEr@YbNd double ratiometric optical nanothermometer *Nanoscale* **8** 5037–42
- [103] Wang S, Westcott S and Chen W 2002 Nanoparticle luminescence thermometry *J. Phys. Chem. B* **106** 11203–9
- [104] Marciniak L, Bednarkiewicz A, Kowalska D and Stręk W 2016 New generation of highly sensitive luminescent thermometers operating in optical window of biological tissues *J. Mater. Chem. C* **4** 5559–63
- [105] Souza A S *et al* 2016 Highly-sensitive Eu³⁺ ratiometric thermometers based on excited state absorption with predictable calibration *Nanoscale* **8** 5327–33
- [106] Eldridge J I, Bencic T J, Allison S W and Beshears D L 2004 Depth-penetrating temperature measurements of thermal barrier coatings incorporating thermographic phosphors *J. Therm. Spray Technol.* **13** 44–50
- [107] Brübach J, Dreizler A and Janicka J 2007 Gas compositional and pressure effects on thermographic phosphor thermometry *Meas. Sci. Technol.* **18** 764–70
- [108] Ranson R M, Thomas C B and Craven M R 1998 A thin film coating for phosphor thermography *Meas. Sci. Technol.* **9** 1947–50
- [109] Mannik L, Brown S K and Campbell S R 1987 Phosphor-based thermometry of rotating surfaces *Appl. Opt.* **26** 4014–7
- [110] Rakov N, Vieira S A, Silva Q P S and Maciel G S 2015 Facile fabrication of Eu³⁺-doped lanthanum oxyfluoride powders by combustion processes and temperature analysis of its fluorescence for thermal sensor application *Sensors Actuators B* **209** 407–12
- [111] Kissel T, Brübach J, Euler M, Frotscher M, Litterscheid C, Albert B and Dreizler A 2013 Phosphor thermometry: On the synthesis and characterisation of Y₃Al₅O₁₂:Eu (YAG:Eu) and YAlO₃:Eu (YAP:Eu) *Mater. Chem. Phys.* **140** 435–40
- [112] West G A and Clements N S 1992 A comparison of the Eu³⁺ temperature dependent emission lifetimes in Sc₂O₃, Y₂O₃ and Gd₂O₃ host crystals *J. Lumin.* **54** 245–8
- [113] Yáñez-González Á, Ruiz-Trejo E, van Wachem B, Skinner S, Beyrau F and Heyes A 2015 A detailed characterization of BaMgAl₁₀O₁₇:Eu phosphor as a thermal history sensor for harsh environments *Sensors Actuators A* **234** 339–45
- [114] Nebatti A, Pflitsch C, Eckert C and Atakan B 2010 Sol–gel-deposition of thin TiO₂:Eu³⁺ thermographic phosphor films *Prog. Org. Coat.* **67** 356–60
- [115] Cates M R, Beshears D L, Allison S W and Simmons C M 1997 Phosphor thermometry at cryogenic temperatures *Rev. Sci. Instrum.* **68** 2412–7
- [116] Chambers M D, Rousseve P A and Clarke D R 2008 Luminescence thermometry for environmental barrier coating materials *Surf. Coat. Technol.* **203** 461–5
- [117] Brübach J, Kissel T, Frotscher M, Euler M, Albert B and Dreizler A 2011 A survey of phosphors novel for thermography *J. Lumin.* **131** 559–64
- [118] Särner G, Richter M and Aldén M 2008 Investigations of blue emitting phosphors for thermometry *Meas. Sci. Technol.* **19** 125304
- [119] Cates M R, Allison S W, Jaiswal S L and Beshears D L 2002 YAG:Dy and YAG:Tm fluorescence above 1400 C *Oak Ridge Natl. Lab. ORNL/TM-2002/71* 1–11
- [120] Eckert C, Pflitsch C and Atakan B 2010 Sol–gel deposition of multiply doped thermographic phosphor coatings Al₂O₃:(Cr³⁺, M³⁺) (M = Dy, Tm) for wide range surface temperature measurement application *Prog. Org. Coat.* **67** 116–9
- [121] McCormack J S 1981 Remote optical measurement of temperature using luminescent materials *Electron. Lett.* **17** 630–1
- [122] Shen Y and Bray K L 1998 Effect of pressure and temperature on 4f–4f luminescence properties of Sm²⁺ ions in M FCl crystals (M = Ba, Sr, and Ca) *Phys. Rev. B* **58** 11944–58
- [123] Cavalli E, Boutinaud P, Mahiou R, Bettinelli M and Dorenbos P 2010 Luminescence dynamics in Tb³⁺-doped CaWO₄ and CaMoO₄ crystals *Inorg. Chem.* **49** 4916–21
- [124] Chambers M D and Clarke D R 2007 Terbium as an alternative for luminescence sensing of temperature of thermal barrier coating materials *Surf. Coat. Technol.* **202** 688–92
- [125] Zhang Z Y, Grattan K T V, Palmer A W and Meggitt B T 1997 Potential for temperature sensor applications of highly neodymium-doped crystals and fiber at up to approximately 1000 °C *Rev. Sci. Instrum.* **68** 2759–63
- [126] Grattan K T V, Manwell J D, Sim S M L and Willson C A 1987 Lifetime investigation of fluorescence from neodymium: Yttrium aluminium garnet at elevated temperatures *Opt. Commun.* **62** 104–7
- [127] Thornton J R, Fountain W D, Flint G W and Crow T G 1969 Properties of neodymium laser materials *Appl. Opt.* **8** 1087–102
- [128] Streck W, Gzafrański C, Łukowiak E, Mazurak Z and Jeżowska-Trzebiatowska B 1977 Fluorescence quenching in neodymium pentaphosphate *Phys. Status Solidi* **41** 547–53
- [129] Dowell L J 1992 Fluorescence thermometry *Appl. Mech. Rev.* **45** 253–60
- [130] Ranson R M, Evangelou E and Thomas C B 1998 Modeling the fluorescent lifetime of Y₂O₃:Eu *Appl. Phys. Lett.* **72** 2663–4
- [131] Allison S, Goedeke S, Cates M, Hollerman W, Eldridge J and Bencic T 2005 *Fluorescence Rise Time Measurements for High Temperature Fluorescence-Based Thermometry* (Oak Ridge, TN: United States Department of Energy)
- [132] Khalid A H and Kontis K 2009 2D surface thermal imaging using rise-time analysis from laser-induced luminescence phosphor thermometry *Meas. Sci. Technol.* **20** 025305
- [133] Lojpur V, Antić Ž and Dramićanin M D 2014 Temperature sensing from the emission rise times of Eu³⁺ in SrY₂O₄ *Phys. Chem. Chem. Phys.* **16** 25636–41
- [134] Li X, Wei X, Qin Y, Chen Y, Duan C and Yin M 2016 The emission rise time of BaY₂ZnO₅:Eu³⁺ for non-contact luminescence thermometry *J. Alloys Compd.* **657** 353–7
- [135] Hao J, Zhang Y and Wei X 2011 Electric-induced enhancement and modulation of upconversion photoluminescence in epitaxial BaTiO₃:Yb/Er thin films *Angew. Chem., Int. Ed.* **50** 6876–80
- [136] Nunez N O, Rivera S, Alcantara D, de la Fuente J M, Garcia-Sevillano J and Ocana M 2013 Surface modified Eu:GdVO₄ nanocrystals for optical and MRI imaging *Dalton Trans.* **42** 10725–34

- [137] Kang X, Yang D, Dai Y, Shang M, Cheng Z, Zhang X, Lian H, Ma P and Lin J 2013 Poly(acrylic acid) modified lanthanide-doped GdVO₄ hollow spheres for up-conversion cell imaging, MRI and pH-dependent drug release *Nanoscale* **5** 253–61
- [138] Gavrilović T V, Jovanović D J, Lojpur V and Dramićanin M D 2014 Multifunctional Eu³⁺- and Er³⁺/Yb³⁺-doped GdVO₄ nanoparticles synthesized by reverse micelle method *Sci. Rep.* **4** 4209
- [139] Singh S K, Kumar K, Srivastava M K, Rai D K and Rai S B 2010 Magnetic-field-induced optical bistability in multifunctional Gd₂O₃:Er³⁺/Yb³⁺ upconversion nanophosphor *Opt. Lett.* **35** 1575–7
- [140] Marciniak L, Waszniewska K, Bednarkiewicz A, Hreniak D and Strek W 2016 Sensitivity of a nanocrystalline luminescent thermometer in high and low excitation density regimes *J. Phys. Chem. C* **120** 8877–82